remote sensing

MDPI

Article

Aboveground Biomass Estimation of Highland Barley in Qinghai–Tibet Plateau—Exploring the Advantages of Time Series Data and Terrain Effects

Jingbo Hu [1,2], Xin Du [1,2,3,*], Qiangzi Li [1,2,4], Yuan Zhang [1,2], Hongyan Wang [1,2], Jingyuan Xu [1,2], Jing Xiao [1,2], Yunqi Shen [1,2], Yong Dong [1,2], Haoxuan Hu [1,2], Sifeng Yan [1,2] and Shuguang Gong [1,2]

1 Aerospace Information Research Institute, Chinese Academy of Sciences, Beijing 100101, China; hujingbo24@mails.ucas.ac.cn (J.H.); liqz@aircas.ac.cn (Q.L.); zhangyuan@aircas.ac.cn (Y.Z.); wanghy@aircas.ac.cn (H.W.); xujingyuan22@mails.ucas.ac.cn (J.X.); xiaojing221@mails.ucas.ac.cn (J.X.); shenyunqi21@mails.ucas.ac.cn (Y.S.); dongyong22@mails.ucas.ac.cn (Y.D.); huhaoxuan23@mails.ucas.ac.cn (H.H.); yansifeng23@mails.ucas.ac.cn (S.Y.); gongshuguang23@mails.ucas.ac.cn (S.G.)
2 University of Chinese Academy of Sciences, Beijing 100049, China
3 School of Mining and Geomatics Engineering, Hebei University of Engineering, Handan 056038, China
4 College of Environment and Planning, Henan University, Kaifeng 475004, China
* Correspondence: duxin@aircas.ac.cn

Abstract: The timely and precise estimation of crop aboveground biomass (AGB) is crucial for evaluating crop development and forecasting yields. The objective is to examine the differences, advantages, and limitations between time series parameters and single-time-phase indicators derived from various vegetation indices in AGB estimation. Moreover, we aim to quantitatively investigate and elucidate the impact of the topographic and geographic conditions of the study region on the estimation of highland barley AGB. Results indicate that AGB simulations utilizing time series parameters from vegetation index time series (VI-TS) curves yield satisfactory results for all three VIs, with the exception of the Normalized Difference Vegetation Index (NDVI), which encounters saturation issues. The performance metrics are as follows: the Enhanced Vegetation Index (EVI) (R^2 = 0.73, RMSE = 20.24 g/m^2), the Soil-Adjusted Vegetation Index (SAVI) (R^2 = 0.67, RMSE = 20.97 g/m^2), and the Normalized Difference Mountain Vegetation Index (NDMVI) (R^2 = 0.54, RMSE = 24.92 g/m^2). The inclusion of our quantitative terrain factor improves the simulation accuracies of NDVI, SAVI, and NDMVI. Overall, the terrain factor has a beneficial impact on the highland barley AGB simulation outcomes. This study establishes a foundational framework for the timely and precise estimation of highland barley biomass, crucial for monitoring agricultural production in plateau mountainous regions.

Keywords: highland barley; biomass estimation; single-time-phase indicators; time series; terrain; vegetation indices

check for updates

Academic Editor: Kun Jia

Received: 8 January 2025
Revised: 2 February 2025
Accepted: 11 February 2025
Published: 14 February 2025

Citation: Hu, J.; Du, X.; Li, Q.; Zhang, Y.; Wang, H.; Xu, J.; Xiao, J.; Shen, Y.; Dong, Y.; Hu, H.; et al. Aboveground Biomass Estimation of Highland Barley in Qinghai–Tibet Plateau—Exploring the Advantages of Time Series Data and Terrain Effects. *Remote Sens.* **2025**, *17*, 655. https://doi.org/10.3390/rs17040655

Copyright: © 2025 by the authors. Licensee MDPI, Basel, Switzerland. This article is an open access article distributed under the terms and conditions of the Creative Commons Attribution (CC BY) license (https://creativecommons.org/licenses/by/4.0/).

1. Introduction

AGB serves as a critical agronomic indicator for crop growth, farm management guidance, and grain yield prediction [1,2], essential for national food security and global carbon dynamics research [3]. Accurate, rapid, and non-destructive insights into the spatial and temporal dynamics of crop AGB are vital for informed field management and yield forecasting. Traditional AGB measurement methods involve destructive sampling [4,5], which, despite high data accuracy, suffer from low efficiency, limited coverage, cumbersome processes, and lack of continuous monitoring, hindering timely regional crop growth

assessment. Since the 1970s, remote sensing has become increasingly pivotal in spatially interpolating and predicting crop AGB, enabling swift, extensive feature information acquisition [6,7]. This technology has been extensively applied to estimate yield, biomass, and other crop parameters, such as for maize, wheat, and rice [8,9]. The advancement of crop AGB estimation through remote sensing is a significant research area in agricultural technology, enhancing precision in agricultural data and crop growth detection capabilities, thereby contributing profoundly to the evolution and utilization of agricultural information technology.

AGB cannot be directly measured from air or space, so the remote sensing approaches for estimating AGB are developed through linking the information derived from remotely sensed data to AGB values measured on the ground. This process typically involves various band combinations used to establish relationships with crop biophysical and ecophysiological parameters, such as leaf area index and chlorophyll content [10]. Generally, methods linking remote sensing data with AGB measurements fall into two categories: empirical modeling and physical modeling. Empirical modeling primarily establishes linear or nonlinear correlations between predictive variables from remote sensing data and AGB field measurements [11–14]. This involves mathematical statistical methods, like correlation analysis, to uncover patterns within the data. These methods range from simple linear regression [15] to complex machine learning algorithms [16]. Common empirical models often use vegetation indices or spectral reflectance data due to their accessibility and ease of computation. However, these indices and data can be influenced by factors such as terrain shadowing, adjacency effects (reflections from nearby terrain), and sky obstruction, which are sometimes overlooked in large-scale applications [17]. Physical models include crop growth models (CGMs) and light energy utilization models. CGMs are based on the physiological and ecological mechanisms of crop growth, considering factors like soil, atmosphere, and irrigation to simulate the crop growth process [18]. The foundation of the light energy utilization model is the net primary productivity (NPP) estimation model, which calculates crop biomass by combining NPP accumulation and respiratory consumption [19]. The primary advantage of this model lies in its clear principles and the requirement for fewer covariates. Among various machine learning algorithms, the emerging Random Forest (RF) algorithm proposed by Leo Breiman and Cutler Adele in 2001 has been regarded as one of the most precise prediction methods for classification and regression, as it can model complex interactions among input variables and is relatively robust in regard to outliers. Random Forest Regression (RFR) achieves precise predictions by constructing multiple decision trees and aggregating their outcomes [20]. It utilizes a bootstrap resampling approach to extract samples from the original data with replacement, forming a training set for the decision trees. Each decision tree grows independently, and the results of multiple trees are combined and aggregated to produce the final prediction. This ensemble approach renders RFR less susceptible to overfitting and highly accurate in handling nonlinear regression tasks. Numerous studies have demonstrated the accuracy and effectiveness of RFR in estimating crop AGB [8,13].

Remotely sensed vegetation indices (VIs), such as the Normalized Difference Vegetation Index (NDVI) and the Enhanced Vegetation Index (EVI), are representative indices for crop aboveground biomass and productivity. Previous studies often rely on single remote sensing images from one single growing season or sampling stage, deriving single-time-phase vegetation index (VI) metrics to construct empirical models for AGB estimation. This approach can lead to issues with data saturation (where VIs fail to distinguish high biomass levels) and systematic errors in the model, such as overestimation of low biomass values and underestimation of high biomass values, resulting in reduced precision [14]. One of the widely used original VI variables is measured during the peak season at the onset of

the reproductive phase, representing the maximum crop green leaf area/biomass. It has been found to reflect a significant correlation between crop VI time series and biomass or yield, providing a generalized way to predict crop biomass or yield [21–23]. However, crop planting dates and phenology vary with location and year, leading to inconsistencies in the timing of the maximum correlation between VI time series and crop biomass across different regions and years. Utilizing a fixed calendar date in the time series to construct remote sensing-based prediction models fails to fully capture the seasonal information from multi-temporal remote sensing imagery and the phenological details embedded in the time series data, rendering this approach suboptimal [24,25]. Dymond et al. [26] suggested that leveraging seasonal time series data could enhance vegetation growth monitoring accuracy. The use of coarse-resolution seasonal time series data from sources like Moderate Resolution Imaging Spectroradiometer (MODIS), Advanced Very High Resolution Radiometer (AVHRR), and SPOT-Vegetation (SPOT-VGT) for large-scale AGB estimation has been investigated [27], with further advancements by subsequent researchers. Zhu and Liu [14] utilized various seasonal Landsat-NDVI-TS data to estimate AGB in southeastern Ohio forests through six empirical modeling methods, finding that seasonal NDVI time series data correlated more strongly with AGB than data from a single peak growing season. Similarly, Prasad et al. [28] highlighted the significance of crop phenology in yield estimation by using phenology indicators derived from filtered, smoothed 16-day synthetic MODIS-NDVI curves to predict regional cotton yields. However, the spatial resolution limitations of these images often overlook the detailed spatial variability of AGB in vegetation. Perry et al. [29] used time-integrated NDVI, a phenological indicator derived from the Sentinel-2 NDVI-TS, to estimate AGB, with R^2 values for measured and estimated AGB ranging from 0.79 to 0.98. Tefera et al. [30] demonstrated a correlation between time-integrated NDVI and pea biomass.

Given the minimal variations in crop varieties and management practices, spatial differences in soil moisture, temperature, solar radiation, organic matter content, and texture—largely influenced by topography—emerge as critical variables in determining crop growth. These factors also account for differences in physiological indicators such as yield and biomass. Topography's impact on temperature and radiation is a primary driver of plant growth variability [31]. Additionally, microclimates formed by diverse hydrothermal characteristics in regions with complex topography significantly influence crop growth [32,33]. The interplay between topography and yield has been thoroughly investigated, with studies examining yield disparities across specific slopes. For instance, Mahler et al. observed higher pea yields on bottom slopes compared to ridge tops and south-facing slopes [34]. Additionally, Kravchenko and Bullock [35] found that topographic elements like elevation, slope, and curvature accounted for 6–54% of yield variability. Notably, these studies focused on statistical analyses of crop yields and topographic conditions without delving into the relationship between biomass and topography. Complex terrain significantly influences variables such as solar radiation, temperature, and, consequently, germination, tiller production, and crop growth [36]. Therefore, a comprehensive investigation into the impact of topographic information on biomass can enable agricultural producers to more accurately monitor crop growth conditions. While numerous studies have examined the relationship between biomass and slope position and have elucidated the connections between biomass and factors such as slope and aspect, the practical application in agricultural production is limited. This limitation arises from the characteristics of sloping arable land, which include issues with water runoff, fertilizer loss, and soil erosion, resulting in a minimal proportion of sloping land cultivation. Even in the Qinghai–Tibet Plateau (QTP), 33.27% of the farmland lies on the flat terrains of the 'One River and Two Rivers' watershed and the Hehuang Valley [37]. The micro-topographic variations

within these farmlands are minimal, suggesting that biomass monitoring should account for the influence of surrounding topographic changes on agricultural output. In such regions, it is crucial to consider the effects of topographic shifts near farmlands to more thoroughly support the evaluation of sustainable agricultural development.

In the QTP, the limited arable land resources coupled with a significant population increase in recent years have resulted in a stark disparity between food production and demand. This imbalance has led to a decline in the region's food self-sufficiency rate. In 2015 alone, the entire QTP faced a food deficit of nearly 1.15 Mt, with certain areas experiencing severe shortages, as reported by Shi et al. [38]. Highland barley is the principal cereal crop over the QTP. Highland barley has been cultivated on the QTP over the past 3500 years and is the main grain crop in the region, providing food for both local humans and livestock. Highland barley, which is the only crop that can grow at elevations of 4200–4500 m, is mainly cultivated in the southern and eastern parts of the QTP [39]. In 2017, the area of cultivated highland barley on the QTP was 2.3×10^3 km^2, representing over 30% of the total crop acreage [39]. Therefore, accurate monitoring and assessment of highland barley yield and biomass parameters on the QTP are crucial for enhancing grain yields and ensuring regional food security. AGB is a key indicator of crop growth status, reflecting photosynthetic efficiency and nutrient accumulation, which directly influence final yield [40]. It also plays an important role in agricultural ecosystem management, livestock feed supply, carbon cycle research, and climate change assessment. By monitoring AGB, it is possible to predict yields more accurately and optimize field management practices, thereby improving the production potential of highland barley.

In summary, the primary objectives of this study are delineated as follows:

Comparative Analysis: To examine the differences, strengths, and weaknesses of single-time-phase indicators versus time series remote sensing parameters for estimating crop AGB using Sentinel-2 imagery with high temporal and spatial resolution;

Dynamic Monitoring: To utilize time series vegetation index data for AGB estimation at any stage or specific moment within the crop growth cycle, enabling rapid monitoring of crop development;

Topographic Impact Assessment: To integrate quantified topographic surface factors into our model and assess the influence of topography on AGB estimation, providing a reference for monitoring agricultural production in regions with complex terrain, such as highland mountains.

2. Materials and Methods

2.1. Study Area

The study area of this research is located in the QTP, which spans from 25°20′N to 39°30′N latitude and 73°20′E to 104°20′E longitude (Figure 1). As the highest plateau globally, it is often referred to as "the Third Pole of the Earth" due to its extreme elevation and environmental significance. Covering approximately 2.57×10^6 km^2, the Qinghai–Tibet Plateau stretches over the whole area of Tibet Autonomous Region and Qinghai Province and parts of Sichuan, Yunnan, Gansu Province, and Xinjiang Uygur Autonomous Region. Most of the plateau belongs to arid and semi-arid areas: the northern zone is dominated by arid areas, and the central and southern zones are dominated by semi-humid and humid areas. The climate is complex, featuring low precipitation, intense solar radiation, significant diurnal temperature fluctuations, and a small annual temperature range. In this region, the annual average temperature range is from −5.75 °C to 2.57 °C, and the annual sunshine duration is from 2500 to 3400 h [41]. It is one of the most important alpine agricultural and pastoral areas in the world [42]. Agricultural land primarily lies below 4600 m above sea level, concentrated in the valleys of the Yarlung Zangbo River and its

tributaries as well as the Yellow River and its tributary Huangshui River [43]. Here, the climate supports crop cultivation, with highland barley being the dominant crop. Highland barley, well adapted to the harsh plateau environment, accounts for approximately 43% of the total cultivated area on the Tibetan Plateau [44]. For local residents, it remains an essential staple food [45].

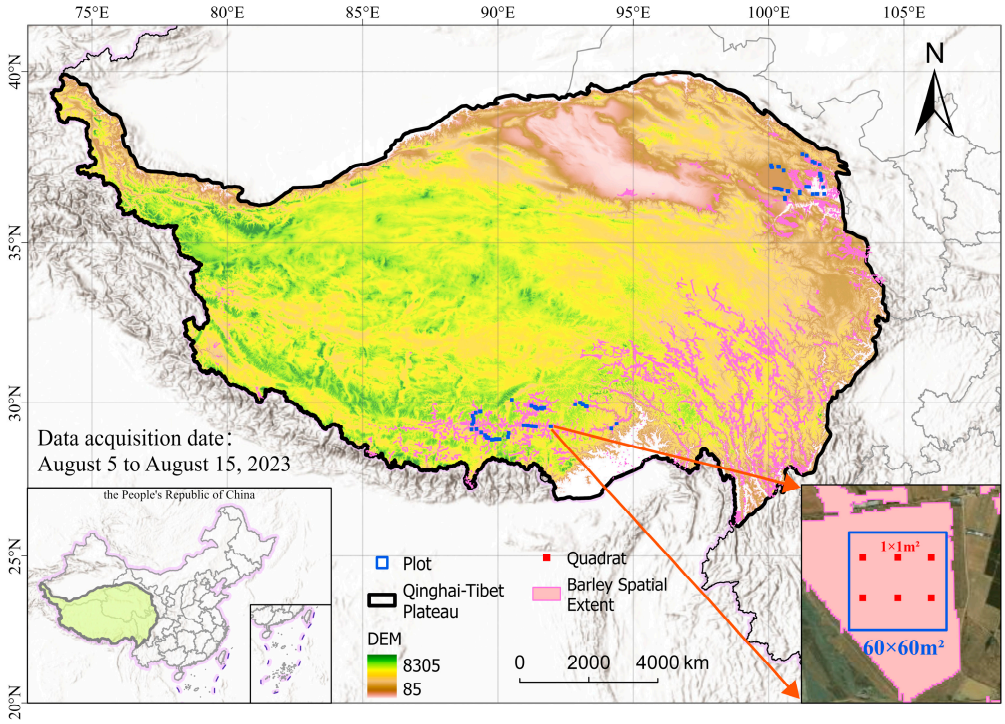

Figure 1. Map of the study area.

2.2. Data Collection

2.2.1. Field Sampling Data

Field experiments for data collection were conducted from 5 August to 15 August 2023, coinciding with the highland barley's maturity stage. The layout of the sample plots, each measuring 60 × 60 m^2, is depicted in Figure 1. Within each plot, six 1 m^2 sample quadrats were established for destructive sampling of all aboveground plant parts, including stems, leaves, and spikes, ensuring the removal of any impurities. The dry matter mass of each sample was determined by subjecting them to drying at a constant temperature of 80 °C for 72 h post greening. The average dry matter mass from the six sample quadrats represented the final AGB value for each plot.

2.2.2. Remote Sensing Data

The Level-2A surface reflectance data set of Sentinel-2 is readily accessible on the Google Earth Engine (GEE, https://earthengine.google.com/, accessed on 10 August 2024) platform. GEE provides up to 10 m resolution visible to shortwave infrared (SWIR) spectral bands in a five-day revisit period. It has undergone radiometric calibration, geometric correction, and atmospheric correction, allowing users to directly utilize it as needed. To maximize the availability of valid time series data for each sampling site, we have utilized all Level-2A images that cover the sampling area from 5 April 2023, to 15 November 2023 (Figure 2). This extensive time frame ensures coverage of the entire highland barley reproductive cycle in the study area.

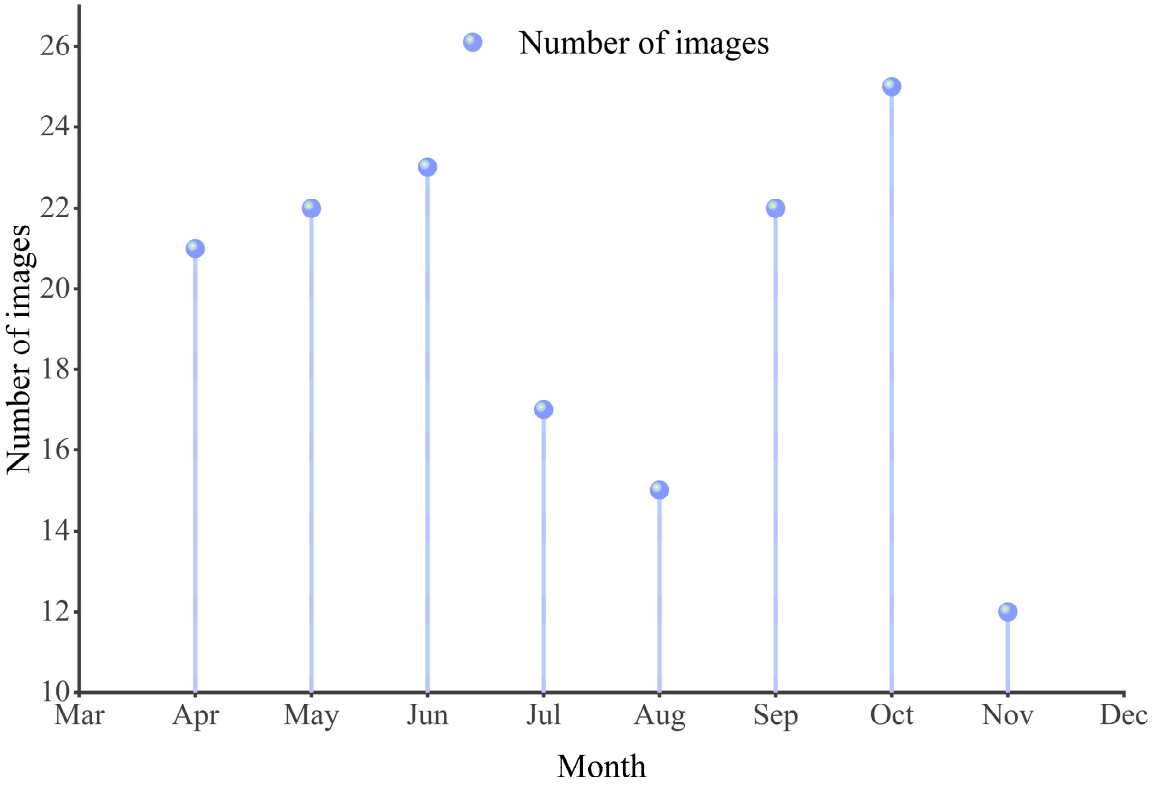

Figure 2. Level-2A imagery covering the sampling area between 5 April 2023, and 15 November 2023.

2.3. Methods

Figure 3 illustrates the workflow of this study, encompassing steps like time series reconstruction, extraction of features from both single-time-phase and time series data, model development, and evaluation of results.

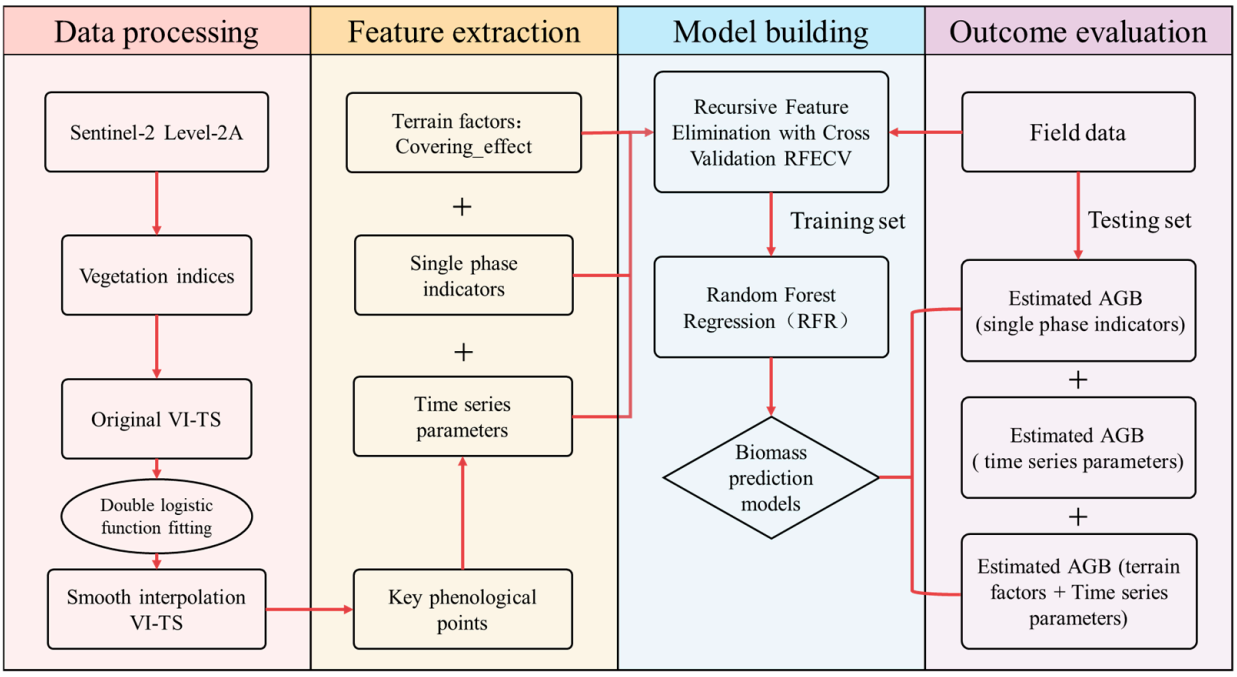

Figure 3. Flow chart.

2.3.1. Data Processing

Vegetation Indices Construction

In this study, we compute a set of vegetation indices (VIs) to develop the AGB estimation model. The definitions of these VIs are detailed in Table 1. Indices like NDVI, SAVI, and EVI are widely utilized to monitor vegetation health. Each index offers unique benefits based on sensor configurations and environmental conditions. NDVI, SAVI, and EVI are particularly noted for their effectiveness in biomass estimation and vegetation monitoring, as supported by several studies [12,46,47]. NDVI, a prevalent VI, gauges vegetation health by measuring the reflectance disparity in the visible and near-infrared spectral bands. While sensitive to chlorophyll levels, making it ideal for crop growth monitoring, NDVI's accuracy can be affected by soil and atmospheric disturbances, as well as saturation in dense biomass regions [48]. To address NDVI's limitations, SAVI incorporates a soil brightness correction factor (L) to reduce soil interference, enhancing its application in areas with sparse vegetation. EVI further refines NDVI to better capture vegetation signals in areas with high biomass and to improve index responsiveness to atmospheric and canopy background variations. In this study, factors such as atmospheric conditions and soil background have been meticulously considered in the application of the aforementioned three types of vegetation indices (VIs). However, one crucial element that cannot be overlooked is the complex topography of the study area. To address this, NDMVI has been incorporated into the analysis to compensate for the influence of terrain factors on traditional VIs and to investigate the impact of topographic correction on the accuracy of highland barley aboveground biomass (AGB) simulation. In this study, the Soil-Adjusted Vegetation Index (SAVI) was calculated using the standard "L" factor of 0.5, which is widely adopted to balance soil noise reduction and vegetation signal preservation. While this value is suitable for general applications, region-specific adjustments to the "L" factor could enhance accuracy in areas with unique soil or vegetation characteristics. Similarly, the Enhanced Vegetation Index (EVI) was computed using the standard MODIS coefficients (L = 1, C1 = 6, C2 = 7.5, and G = 2.5), which are designed to minimize atmospheric and soil background effects. However, optimized parameters tailored to the specific conditions of the study area may improve the performance of EVI in capturing vegetation dynamics. Future studies could explore the calibration of these coefficients to better suit regional characteristics, thereby refining the accuracy of vegetation indices derived from satellite data.

It is worth noting that NDMVI, based on NDVI with terrain correction, aims to reduce or eliminate the influence of terrain effects. Zhu et al. [49] applied cosine correction and C-correction models to mitigate the impact of diffuse irradiance on reflectance, thus reducing terrain effects on VI. They discovered that reflectance in the near-infrared (NIR) and Short-Wave Infrared (SWIR) bands is more susceptible to topographic changes compared to the red band. While the red band's diffuse sky radiation helps even out reflectance variations due to topography, this effect is less pronounced in the NIR and SWIR bands. In mountainous regions, terrain-induced occlusion and multiple scattering can significantly distort spectral data at the pixel level in satellite imagery, with higher spatial resolution images being more affected by topography [50,51]. To counteract the complex terrain's influence, some researchers have suggested a novel approach: maintaining the integrity of spectral curve information while tweaking the Normalized Difference Vegetation Index (NDVI) formula—either by increasing the numerator or decreasing the denominator. This adjustment ensures that the VI enhancement for sunlit slopes is less than that for shaded slopes, bringing the VI values for identical vegetation types on both slopes closer together. This strategy effectively neutralizes topographic disparities, enhancing the precision of VI computation and extraction [52]. Building on this concept, the Normalized Difference

Mountain Vegetation Index (NDMVI) is introduced, which has proven adept at dampening or even nullifying topographic influences.

Table 1. The equations utilized for computing the vegetation indices.

Vegetation Index	Formulation	Reference
NDVI	$\frac{NIR-RED}{NIR+RED}$	[53]
EVI	$\frac{NIR-RED}{NIR+6*RED-7.5*BLUE+1} * 2.5$	[54]
SAVI	$\frac{NIR-RED}{NIR+RED+L} * (1+L)$	[55]
NDMVI	$\frac{(NIR-RED)+(RED_{\min}-NIR_{\min})}{(NIR+RED)-(RED_{\min}+NIR_{\min})}$	[52]

RED is red band reflectance, *NIR* is near-infrared band reflectance, $RED_{\min}$ is the minimum red band reflectance for each image within the sampling region, $NIR_{\min}$ is the minimum near-infrared band reflectance for each image within the sampling region, *BLUE* is the blue band reflectance, and *L* is the soil brightness correction factor.

Vegetation Index Time Series (VI-TS) Reconstruction

VI-TS, derived from satellite data, is extensively used to monitor vegetation's spatial and temporal variations. Yet, several factors, including atmospheric noise, residuals from radiometric corrections, BRDF (bidirectional reflectance distribution function) effects, and topographic effects, obscure the true changes occurring on the ground, impeding the extraction of information from VI-TS. Differences in terrain orientation often create variation in signal values between pixels with similar land cover and biophysical–structural properties due to differences in irradiance (caused by the angle of incident illumination) and radiance (determined by the angle of exitance). This topographic effect has a negative influence on the products derived from remote sensing data [56]. For non-Lambertian surfaces, the reflected radiance is also affected by the intrinsic reflective properties of the surface described by the bidirectional reflectance distribution function (BRDF) [57]. These effects may further lead to variations in vegetation indices. To mitigate these adverse effects and more accurately capture seasonal vegetation–climate characteristics, a time function fitting approach was employed. This method allowed us to reconstruct a high-quality VI-TS and extract both single-time-phase remote sensing data and time series parameters. Although the chosen double logistic (DL) function fitting method is likely to mitigate these issues to some extent, the potential influence of BRDF and topographic effects should still be acknowledged in the analysis.

Given the diversity of VI-TS profiles and the simplicity and flexibility of temporal function fitting methods, we ultimately selected the widely used double logistic (DL) function fitting method. The application of the DL function to VI-TS fitting can be traced back to the work of Fisher et al. [58] who developed a semi-empirical model using five parameters to describe annual NDVI time profiles and successfully applied it to both homogeneous and heterogeneous farmlands. Furthermore, Zhang et al. [59] utilized the curvature change rate based on the DL function to detect phenology and derived relatively accurate phenological transition dates, demonstrating the effectiveness and practicality of the DL function in VI-TS filtering and reconstruction. Zhu et al. [60] proposed a self-weighting function fitting method from curve features (SWCF) based on the DL function, showing that the DL function can adapt to various shapes of VI-TS and is not limited to NDVI alone. As long as the time series curve exhibits a unimodal pattern of rising first and then falling, the DL function can be used for fitting and reconstruction. The four vegetation indices used in this study all follow a single-peak seasonal trajectory, allowing for processing using the same time function fitting method.

The following double logistic function is used to model the process of VI-TS curve variation:

$$f(t) = v_{\min} + \frac{v_1}{1+\exp(m_1+n_1t)} - \frac{v_2}{1+\exp(m_2+n_2t)} \quad (1)$$

where t represents the DOY corresponding to the VI point. $v_{\min}$, v_1, v_2, m_1, n_1, m_2, and n_2 are seven function parameters to be optimized. $v_{\min}$ is the preseasonal background VI value, v_1 is the difference between the peak VI value and the preseasonal background VI value, and v_2 is the difference between the peak VI value and the postseasonal background VI value. m_1 and n_1 represent the peak position and slope of the VI time series curve in the vegetation growth stage, and m_2 and n_2 represent the peak position and slope of the VI time series curve in the vegetation senescence stage, respectively.

Feature Extraction

1. Extraction of Key Phenological Dates During the Vegetation Fertility Period

The VI-TS curves reconstructed with the DL effectively illustrate the gradual dynamics of vegetation growth and seasonal phenology. Four key phenological dates were identified from these curves prior to the sampling date, defining crucial periods of vegetation dynamics annually (see Figure 4). These dates are the following: (1) start of growing season (SOS), the date when the photosynthetic activity of the vegetation begins, which is mathematically interpreted on the fitted curve as the first maximum point of the second-order derivative; (2) the rapid growth point (RGP), the date of fastest growth of the vegetative leaves, which corresponds to the mathematical interpretation of the point of the maximum value of the first-order derivative of the fitted curve; (3) the plateau period (Plateau), the date when the vegetative green leaf area is maximum, where the corresponding mathematical interpretation is the first minimal value point of the second-order derivative of the fitted curve; and (4) Peak point (Peak point), the date corresponding to the peak of the fitted curve. These key dates were derived using the curvature of a fitted DL model and the rate of change in curvature, indicating transitions in the annual cycle from one approximately linear stage to another. Studies on vegetation phenology have demonstrated that these dates effectively characterize key phenological stages of vegetation dynamics during the reproductive period [59,61]. The calculation of these key dates relies solely on the fitted bi-logistic model, objectively characterizing the phenological stage of each sample quadrat. Compared to the traditional growth stages such as tillering, jointing, and filling, these key dates can be accurately calculated to facilitate the extraction of time series parameters and single-time-phase indicators from the smoothed VI-TS curves.

2. Extraction of Time Series (TS) Parameters and Single-Time-Phase Indicators

In "1. Extraction of Key Phenological Dates during the Vegetation Fertility Period", key phenological periods characterizing vegetation dynamics were extracted from the smoothed VI-TS. Based on the literature, we extracted two sets of metrics from the smoothed and interpolated VI-TS to represent the time series parameters (Figure 5) and the single-time-phase indicators (Figure 6) through the key phenological dates.

The single-time-phase indicators primarily indicate the physiological phases of crops during various growth stages, gauged by VI values. Based on the four phenological milestones outlined in "1. Extraction of Key Phenological Dates during the Vegetation Fertility Period", we segmented the crop's pre-sampling growth into four distinct phases, depicted in Figure 6. We computed the mean VI for each phase, establishing it as the stage's unique time-phase index. Consequently, we derived four individual time-phase indicators for every VI.

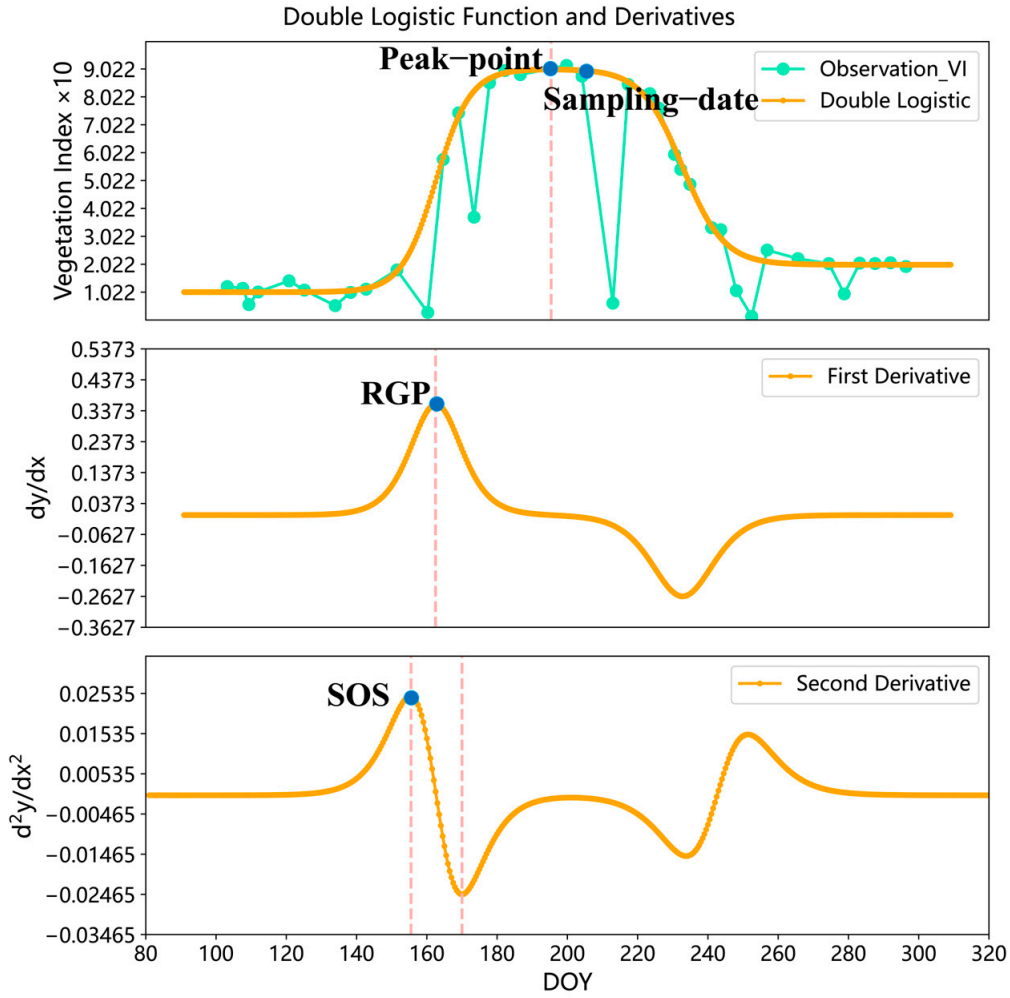

Figure 4. Key phenological dates extracted from VI-TS curves.

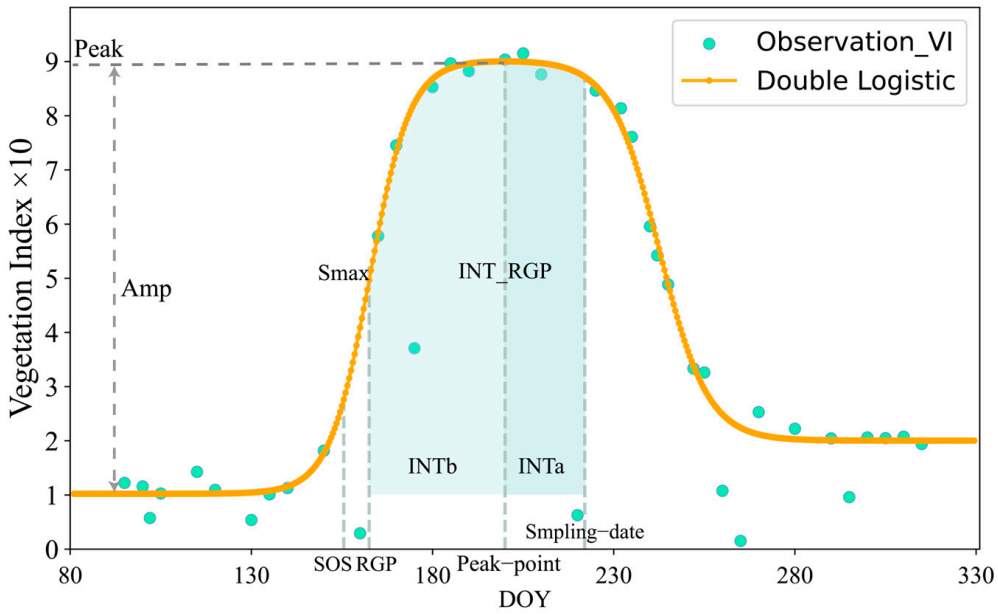

Figure 5. Time series parameters derived from fitted double logistic curves. A portion of the time series parameters extracted from the fitted VI-TS curves is presented.

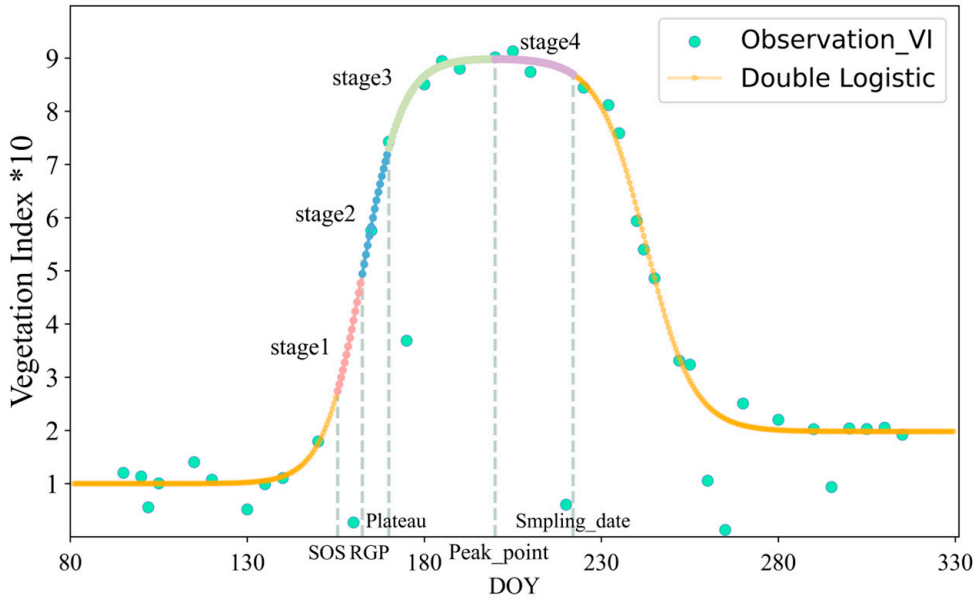

Figure 6. Single-time-phase indicators from fitted double logistic curves. The stage1, stage2, stage3, and stage4 shown in the figure are the single-time-phase indicators extracted according to the phenological period.

3. Terrain Parameter Extraction

To mitigate the influence of geographic variability on aboveground biomass (AGB) estimation within the study area, NDMVI was introduced to counteract terrain effects. However, NDMVI, derived from secondary development of NDVI and subjected to a series of treatments such as smoothing and interpolation, reflects limited terrain effects. Moreover, NDMVI is designed to correct NDVI within sampled agricultural fields and does not consider the influence of surrounding terrain. In 2014, China launched a new phase of the Grain for Green Program. According to official documents, by 2020, all sloping farmland above 25° nationwide will be converted to forests and grasslands [62]. Consequently, the majority of current farmland is situated in areas with relatively gentle terrain, where micro-topographic differences within farmland are minimal. It is therefore imperative to consider the impact of surrounding terrain on agricultural production. Hence, to more accurately reflect the influence of surrounding terrain on aboveground biomass (AGB) estimation, a new terrain factor termed "Covering_effect" was extracted to represent the shielding effect of mountains surrounding farmland on incoming sunlight. The analysis primarily focuses on the impact of southern mountains on the sunlight received by crops. Since solar radiation intensity and the duration of vegetation exposure to light directly affect plant energy utilization efficiency, subsequently influencing net primary productivity and causing changes in growth parameters such as AGB, Covering_effect primarily utilizes high-resolution remote sensing imagery and digital elevation model data for its computation. Its calculation formula is provided below:

$$Covering_effect = \frac{H}{D} \tag{2}$$

where H represents the highest elevation of mountains within a 2 km radius south of each ground sampling point, and D is the straight-line distance between the highest elevation point and the sampling point. The magnitude of Covering_effect indicates the strength of the mountain's shading effect on the farmland. A larger Covering_effect implies a stronger

shading effect, while a smaller one suggests a lesser shading effect on the farmland and thus less impact on the solar energy absorbed by the crops.

The calculated terrain parameters are used as features of each sampling plot for subsequent use in AGB estimation.

2.3.2. Model Training, Validation, and Evaluation

The dimension of the feature vector directly impacts the accuracy of the final estimation, underscoring the importance of identifying the optimal combination of features. Several feature selection methods incorporate the regression model into the selection process, utilizing cross-validation results as evaluation criteria and ultimately selecting feature vectors with high contribution values as optimal solutions. In this study, we employ Recursive Feature Elimination with Cross Validation (RFECV) based on 5-fold cross-validation to determine the optimal feature combination. During RFECV execution, we calculate the average RMSE for each cross-validation iteration across varying numbers of features. We then identify the number of features yielding the smallest RMSE and conduct RFECV using the backward recursive method. Finally, we generate the feature importance ranking of the optimal feature vectors.

To optimize the performance of the RFR model, Grid Search was employed as a systematic method for hyperparameter tuning. Grid Search exhaustively explores a predefined set of hyperparameter combinations to identify the optimal configuration that minimizes the prediction error. The performance of each hyperparameter combination was evaluated using 5-fold cross-validation, with the root mean square error (RMSE) as the evaluation metric. The optimal hyperparameter combination was selected based on the lowest average RMSE across all folds.

This study involves three primary modeling processes for biomass estimation: using single-time-phase indicators, utilizing time series parameters, and incorporating the terrain parameter. The training and validation sets were divided in a 7:3 ratio, with 45 samples in the training set and 20 in the validation set. The first modeling approach eschewed feature selection due to the minimal feature set. Conversely, the second approach, which dealt with an extensive feature set, employed feature selection to ascertain the optimal feature combination and to quantify the significance of each feature. The final modeling process, integrating the terrain parameter, built upon the optimal time series feature combination, further quantifying feature importance to develop an enhanced model.

The root mean square error (RMSE) and the coefficient of determination (R^2) are utilized to evaluate the model's performance. RMSE is a widely adopted metric for evaluating the disparity between the predicted values of the model and the actual observed or measured values. R^2 gauges the proximity of the predicted and measured values of AGB to a 1:1 line, indicating how well the model elucidates the total AGB. Each indicator is defined as follows:

$$RMSE = \sqrt{\frac{\sum_{i=1}^{n} (y_{m,i} - y_{e,i})^2}{n}} \tag{3}$$

$$R^2 = 1 - \frac{\sum_{i=1}^{n} (y_{m,i} - y_{e,i})^2}{\sum_{i=1}^{n} (y_{m,i} - \overline{y_m})^2} \tag{4}$$

where $y_{m,i}$ and $y_{e,i}$ represent the measured and modeled values at sample plot i, respectively, and $\overline{y_m}$ represents the mean of the measured values.

3. Results

3.1. Time Series Curve Reconstruction Results

Figure 7 illustrates the results of reconstructing the four VI-TS using the double logistic function. For computational convenience, the original VI values were linearly stretched, and the linear stretch value was set to 10, following the recommendation of Zhu et al. [60]. At this setting, the reconstruction accuracy of the VI-TS curves achieved through fitting with the DL function is maximized, and the corresponding RMSE reduction rate is the highest [60]. The fitted curve closely approximates the upper envelope of the original VI-TS, accurately capturing seasonal variations in vegetation and surface dynamics while effectively mitigating the influence of VI points contaminated by clouds and atmospheric interference. The DL curve fitting method leverages the temporal information embedded within the time series itself to minimize errors associated with exogenous effects [63]. The efficacy of this fitting approach has been further validated by Zhu et al.

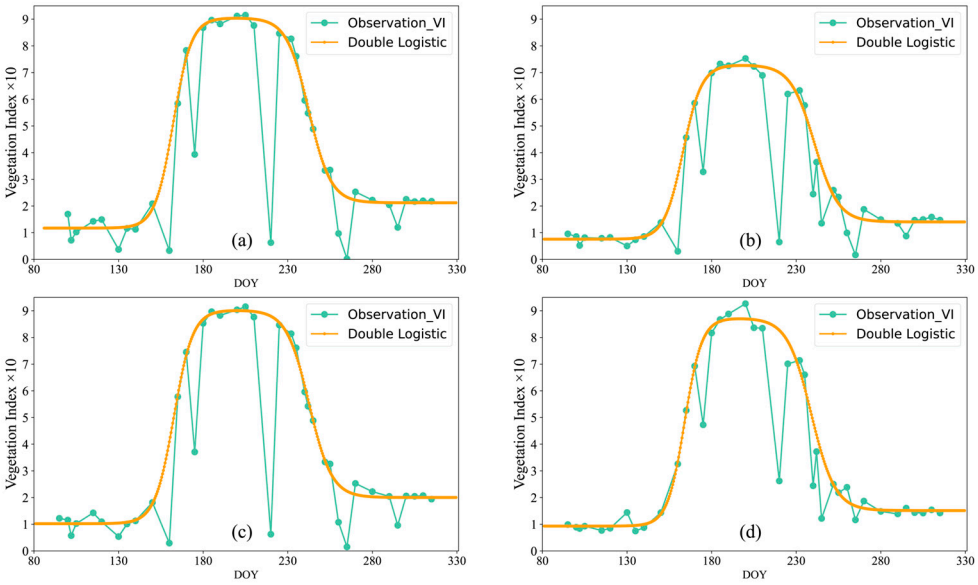

Figure 7. The results of the fitting reconstruction for VI-TS using the DL function are presented. Panels (**a**–**d**) correspond to the time series of NDMVI, SAVI, NDVI, and EVI, respectively.

3.2. Biomass Estimation Using Single-Time-Phase Indicators

Table 2 displays the four growth stages derived from each VI-TS. Utilizing the same growth stage across all VI-TS as a feature vector and considering the limited dimensionality of the feature vector, all features are incorporated for modeling. The relative contributions of different VIs to the construction of the RFR model for each growth stage are depicted in Figure 8. In the initial growth stage, NDVI emerged as the most influential contributor to AGB estimation, accounting for 35%, closely followed by NDMVI at 33%, indicating comparable significance. Subsequent analysis (Figure 8b–d) reveals a consistent trend across the three subsequent growth stages, characterized by rapid crop leaf expansion. Here, EVI consistently exhibited the highest contribution, surpassing 50% in significance, demonstrating superior performance compared to other VIs. Furthermore, the importance of NDVI in AGB inversion exhibited a gradual decline from the second growth stage onwards. Upon reaching the third growth stage, corresponding to the Plateau of crop growth, the importance of NDVI reached its nadir, persisting until the sampling date. Conversely, the significance of SAVI for AGB inversion remained consistently low throughout the entire crop growth cycle preceding the sampling date.

Table 2. Time series parameters and single-time-phase indicators derived from smoothed VI-TS curves used for model construction.

Type	Abbreviation	Definition
Time Series Parameters	VImin	Preseasonal background VI value of the VI-TS curve
	Peak	Maximum value of the VI-TS curve
	Amp	Amplitude of the VI-TS curve
	SOS	Start of growing season
	RGP	The rapid growth point, the date of fastest growth of the vegetative leaves
	Plateau	Plateau period, the date when the vegetative green leaf area is maximum
	Smax	Maximum slope of the VI-TS curve
	INTb	Integration under the VI-TS curve between RGP and peak date
	INTa	Integration under the VI-TS curve between the peak date and the sampling date
	INT_RGP	Integration under the VI-TS curve between RGP and sampling date
	INT_SOS	Integration under the VI-TS curve between SOS and the sampling date
	VI_SOS	VI value corresponding to SOS
	VI_RGP	VI value corresponding to RGP
	VI_Plateau	VI value corresponding to Plateau
	VI_222	VI value corresponding to the sampling date
Single-Time-Phase Indicators	stage1	Mean of VI-TS curve between SOS and RGP
	stage2	Mean of VI-TS curve between RGP and Plateau
	stage3	Mean of VI-TS curve between Plateau and peak date
	stage4	Mean of VI-TS curve between the peak date and the sampling date

After evaluating the contributions of different vegetation indices to AGB inversion at each growth stage, we proceeded to generate a new feature vector using the most significant vegetation index feature from each growth stage and constructed a new model for highland barley AGB simulation. The importance ranking of the new feature vector is depicted in Figure 8e. Overall, EVI contributed more substantially to AGB simulation than NDVI.

The accuracy validation results of the RFR model for simulating AGB using vegetation indices from different growth stages are depicted in Figure 9. Notably, the first growth stage exhibited the poorest AGB simulation performance (R^2 = 0.14, RMSE = 36.57 g/m^2), while the fourth growth stage demonstrated the most accurate AGB simulation (R^2 = 0.46, RMSE = 25.57 g/m^2). This stage falls between the peak date of the VI-TS curve and the sampling date. Furthermore, it is evident from the results that significant saturation occurred in all highland barley AGB simulations using the second, third, and fourth growth stages. Specifically, AGB was notably underestimated when the actual AGB exceeded 1430 g/m^2, while smaller AGB values were severely overestimated. This situation is very similar to that reported by Powell et al. [63]. The likely explanation lies in the fact that the second growth stage is initiated from the rapid growth point (RGP), marking the period of fastest vegetation leaf growth. By the third growth stage, the vegetation leaf area reaches a phenologically defined maximum, resulting in a dense vegetation canopy where the spectral red band reflectance remains relatively unchanged while the near-infrared reflectance continues to increase. Despite some corrections applied to EVI, SAVI, and NDMVI themselves, saturation persists. Conversely, the simulation results for the first growth phase did not exhibit significant saturation, but individual samples displayed considerable simulation deviations (Figure 9a). When AGB simulations were conducted using the most important vegetation index features for each growth stage, the accuracy did not improve, and the same saturation phenomenon persisted (Figure 9e).

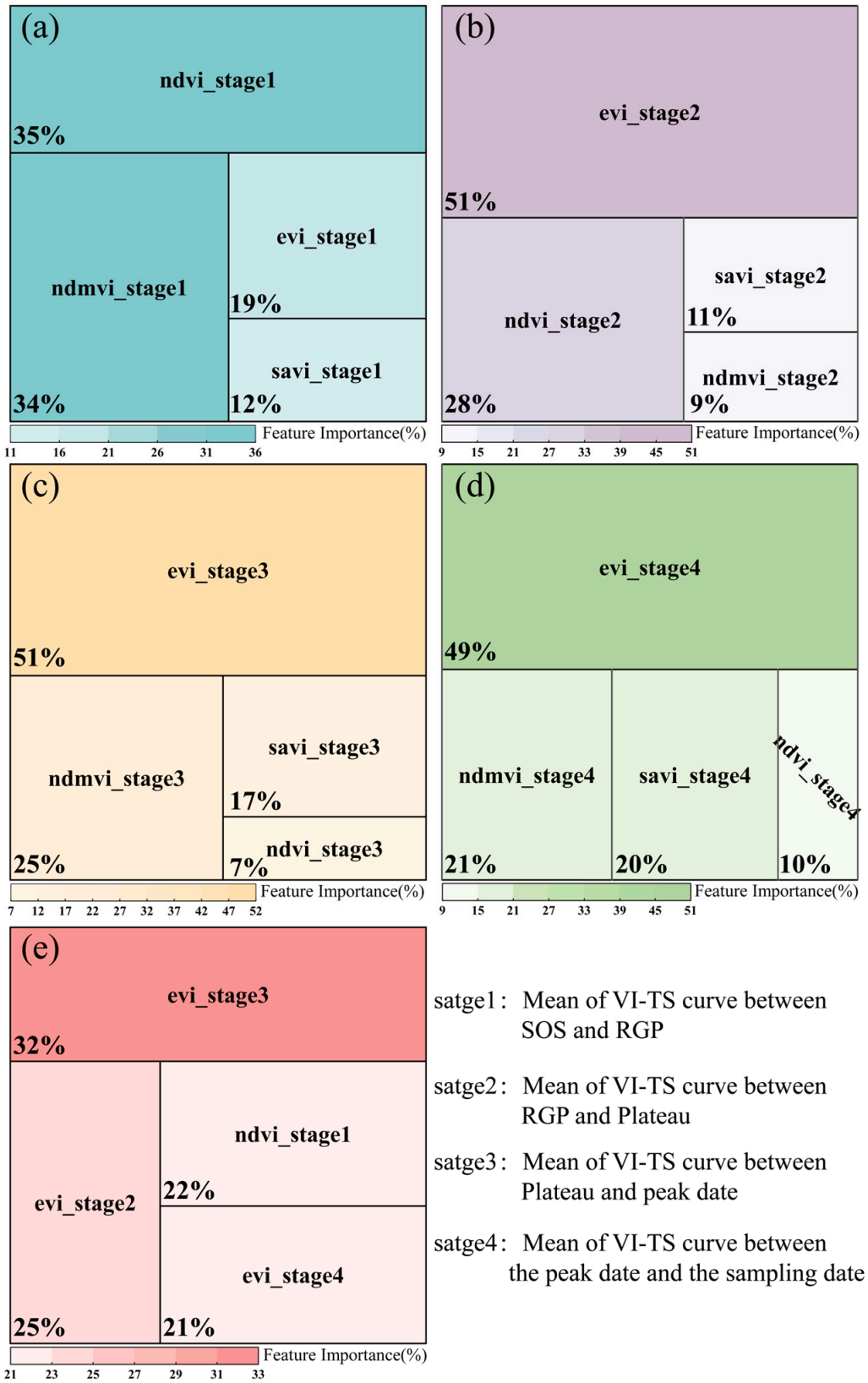

Figure 8. Contribution of each vegetation index to the model at different growth stages. (**a**–**d**) represent the first growth stage, second growth stage, third growth stage, and fourth growth stage, respectively. (**e**) represents the combination of vegetation indices with the highest contribution from each growth stage. Larger areas and darker colors in the figure represent higher importance levels.

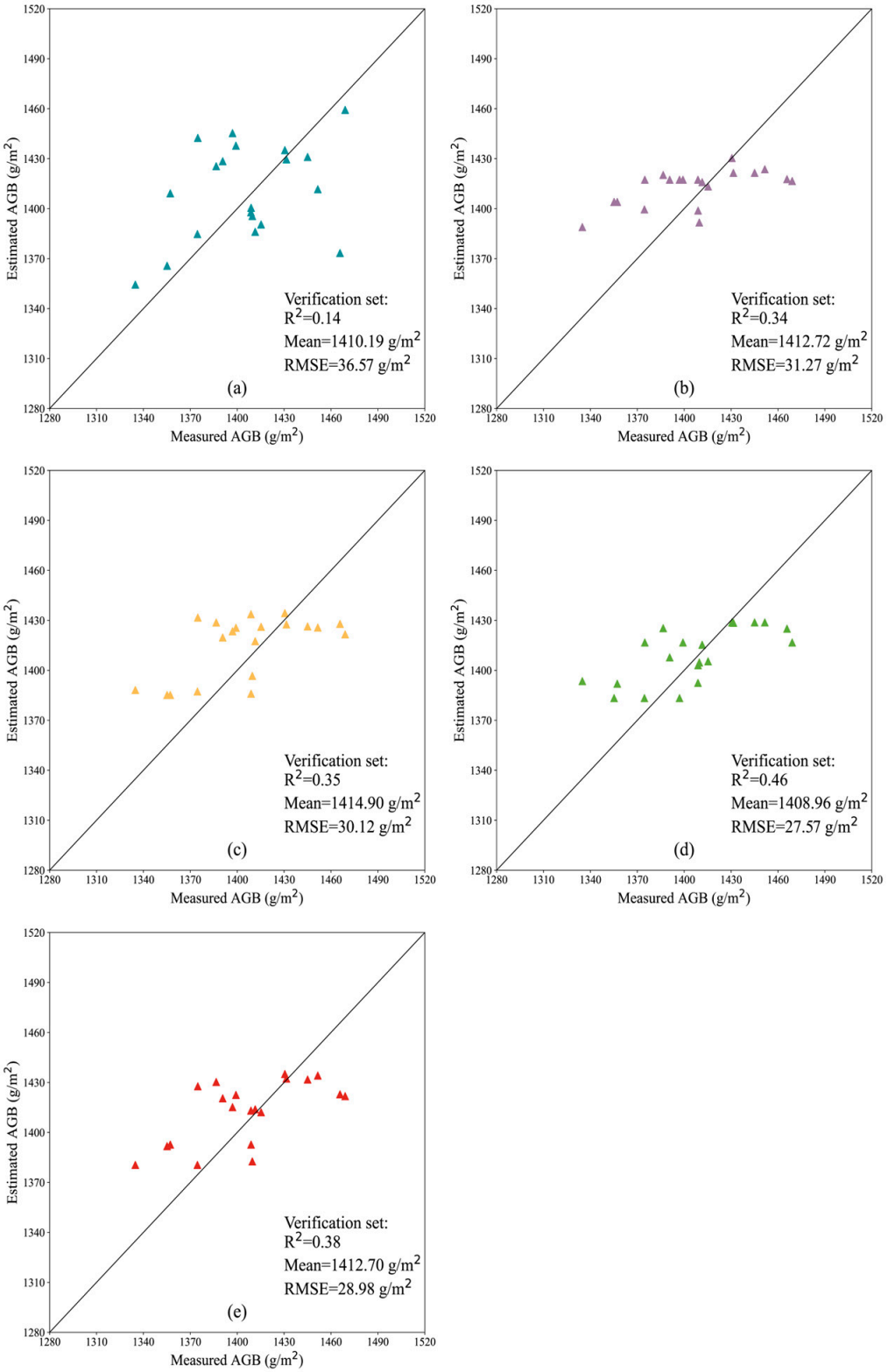

Figure 9. Simulation results of biomass at different growth stages. (**a**–**d**) represent the results of biomass simulations using combinations of vegetation indices for the first growth stage, second growth stage, third growth stage, and fourth growth stage, respectively. (**e**) represents the results of biomass simulations using the combination of vegetation indices with the highest contribution from each growth stage.

3.3. Biomass Estimation Using Vegetation Index Time Series (VI-TS) Parameters

In constructing the RFR model, each VI is characterized by 12 time series parameters. Selecting the appropriate input features for the RFR model is essential to prevent overfitting and to streamline the model. The average RMSE associated with different feature counts was determined using recursive feature elimination (RFE) based on 5-fold cross-validation, as illustrated in Figure 10. The smallest RMSE for each VI indicates the optimal feature vector dimension for modeling with that index. The modeling performance of each VI initially improves and then diminishes as the feature vector dimension increases. Figure 10 also ranks the significance of the optimal features post-filtering. NDMVI and SAVI require the most modeling features, at seven each. In contrast, NDVI and EVI need the fewest, at two each, and exhibit smaller RMSE than NDMVI and SAVI.

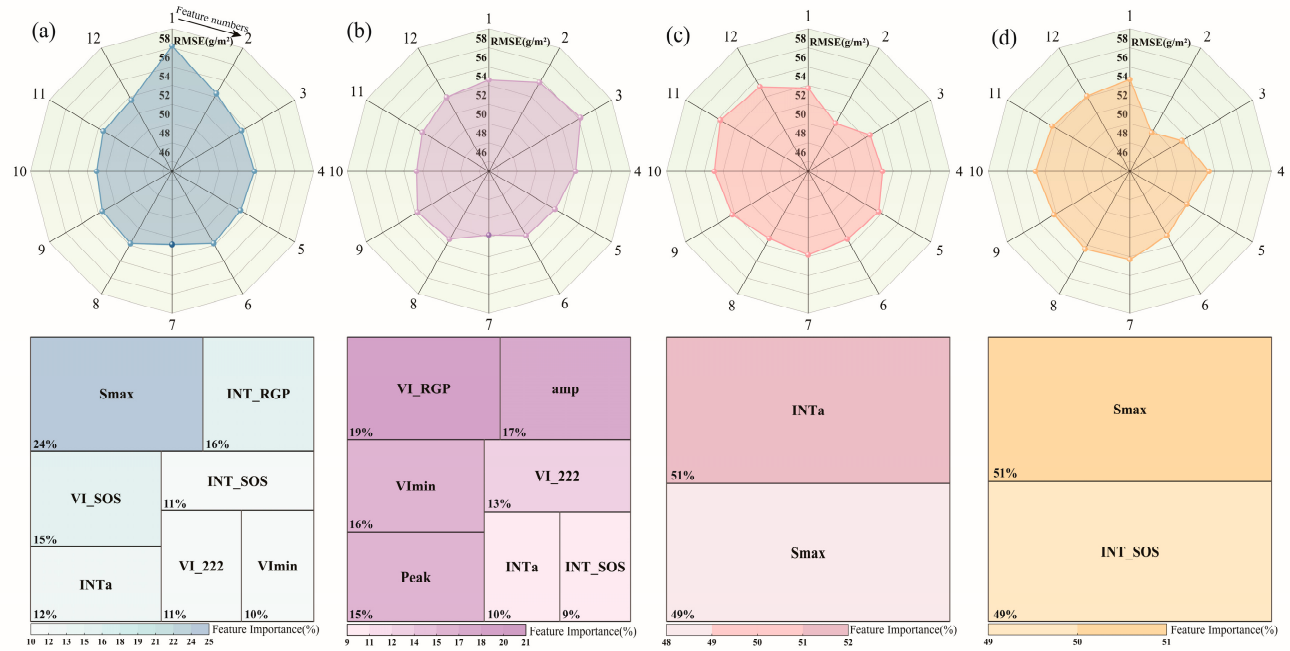

Figure 10. Recursive feature elimination method and importance ranking. (**a**–**d**) represent the results of recursive feature elimination for the time series parameters of NDMVI, SAVI, NDVI, and EVI, respectively.

Figure 11 illustrates the highland barley AGB simulation results for the optimal feature combinations of each vegetation index. In terms of simulation accuracy, EVI exhibited the highest effectiveness (R^2 = 0.73, RMSE = 20.24 g/m^2), followed by SAVI (R^2 = 0.67, RMSE = 20.97 g/m^2). Notably, NDMVI, which integrates a terrain correction factor based on NDVI to mitigate or eliminate terrain effects, enhanced the highland barley AGB simulation accuracy (R^2 = 0.54, RMSE = 24.92 g/m^2), representing a 20% improvement in R^2 and a 12% reduction in RMSE compared to NDVI alone. To further investigate the contribution of terrain effect, we incorporated the covering_effect metric into the modeling process for each vegetation index, as detailed in Section 3.4. Our results indicate that the terrain correction factor in NDMVI plays a significant role in improving simulation accuracy. However, we also acknowledge that the differences between NDMVI and NDVI may partially arise from their distinct equations and band combinations.

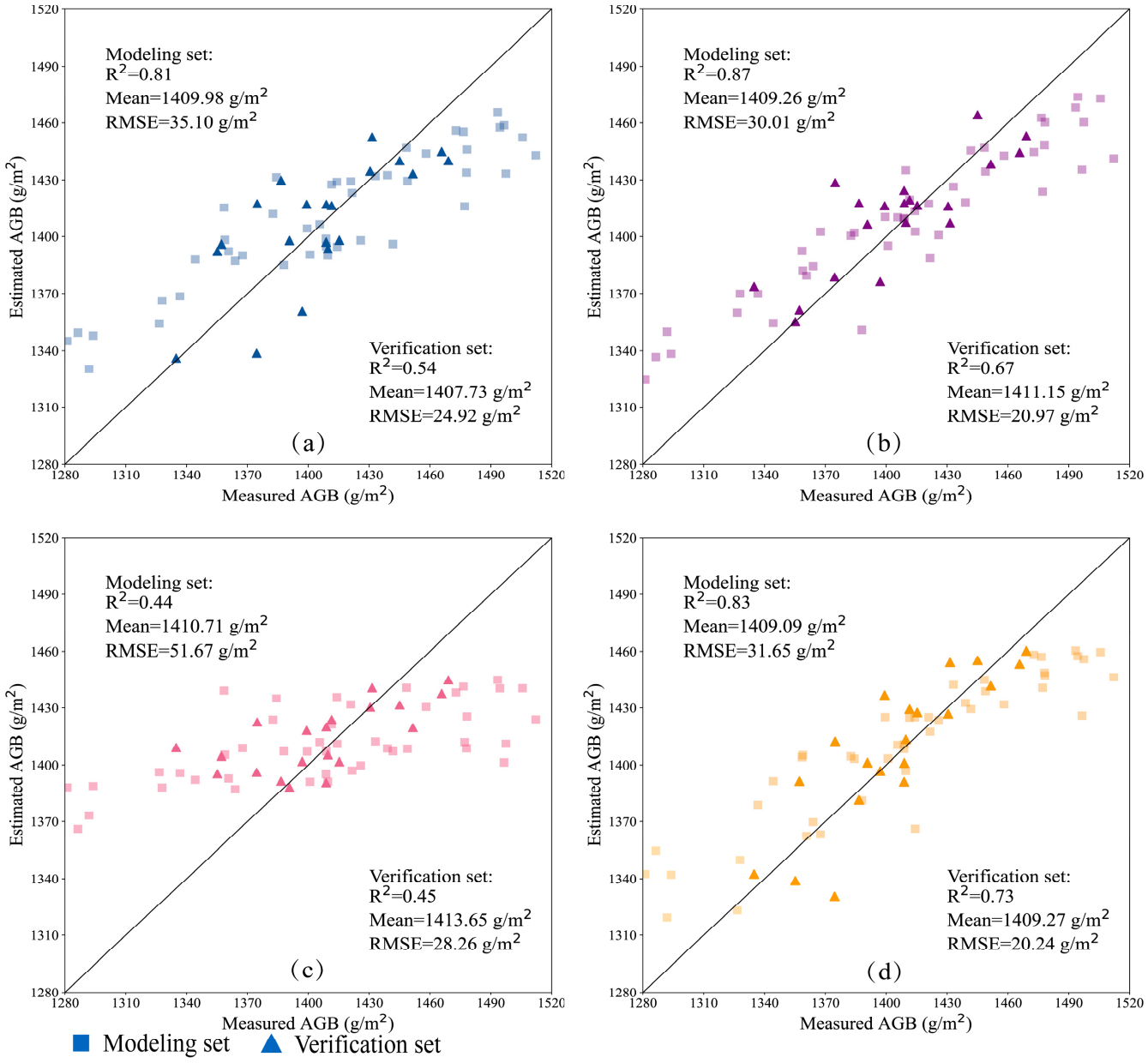

Figure 11. Biomass simulation results using time series parameters. (**a**–**d**) represent the results of biomass simulation using time series parameters of NDMVI, SAVI, NDVI, and EVI, respectively.

3.4. Biomass Estimation by Introducing Terrain Parameter

In Section 3.2, the optimal feature vectors for modeling each vegetation index were identified. Building on this, the terrain parameter, Covering_effect, from "3. Terrain Parameter Extraction" was incorporated into each index's optimal feature vector, labeled as Terrain, to develop a new RFR model. The contribution of each feature to the model is depicted in Figure 12. The Terrain feature consistently exhibits a greater contribution than the others across all three indices—NDMVI, SAVI, and NDVI. However, for the EVI index, the terrain's contribution is less significant compared to the other features.

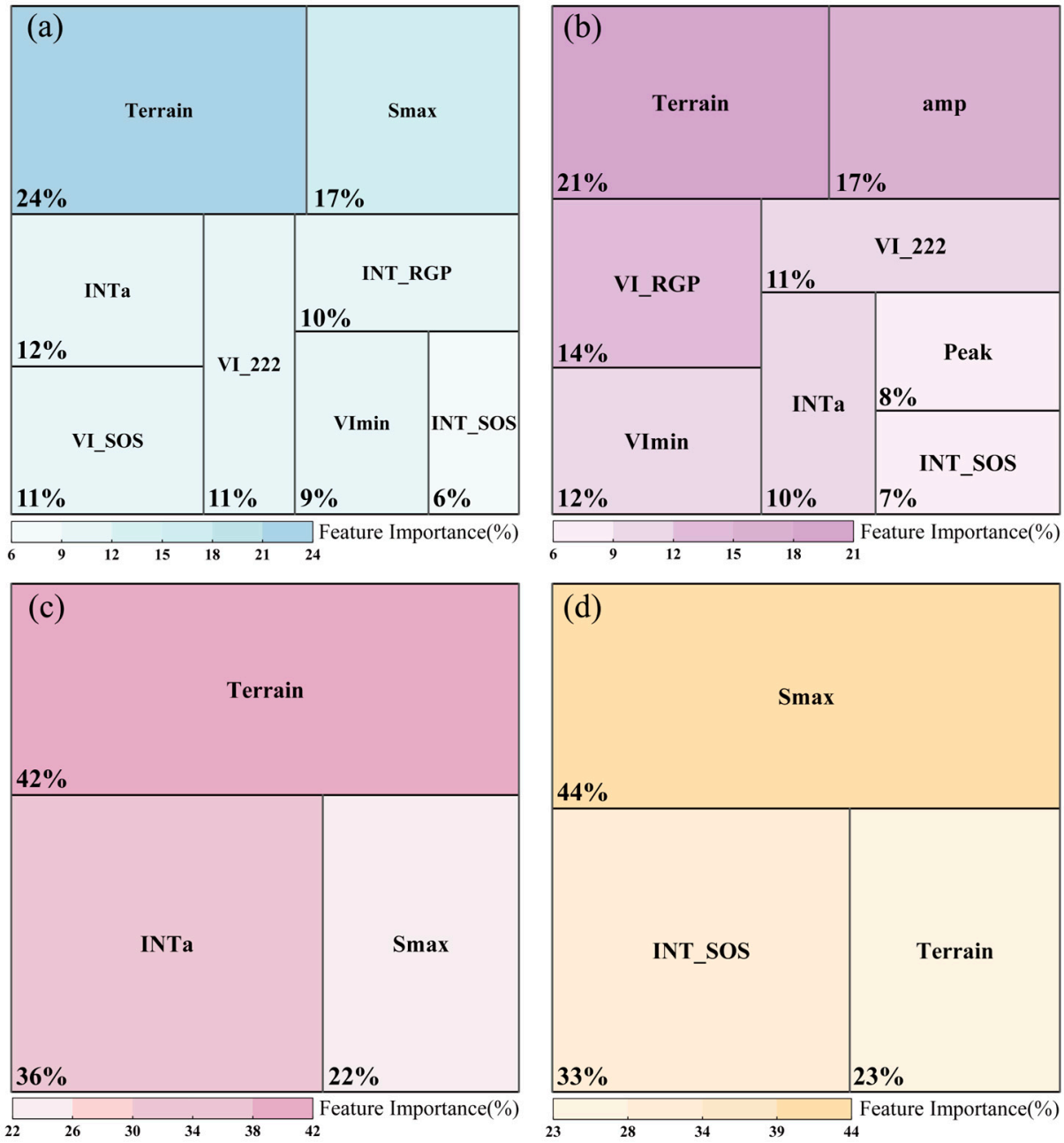

Figure 12. Ranking of feature importance of introduced terrain factors. (**a**–**d**) represent the ordering of the importance of the features after adding terrain factors to the time series parameters of NDMVI, SAVI, NDVI, and EVI, respectively.

Figure 13 illustrates the simulation outcomes for each index after incorporating terrain parameters. Comparing with the simulation results without the terrain parameter in Figure 11, it is evident that the accuracies of NDMVI, SAVI, and NDVI have improved variably. However, the inclusion of the terrain parameter has adversely impacted the EVI simulation, leading to reduced accuracies. Among the four indices, SAVI stands out with the best performance, boasting an R^2 of 0.73 and an RMSE of 20.24 g/m^2. Overall, the integration of terrain parameters has a generally positive effect on the highland barley AGB simulation accuracy.

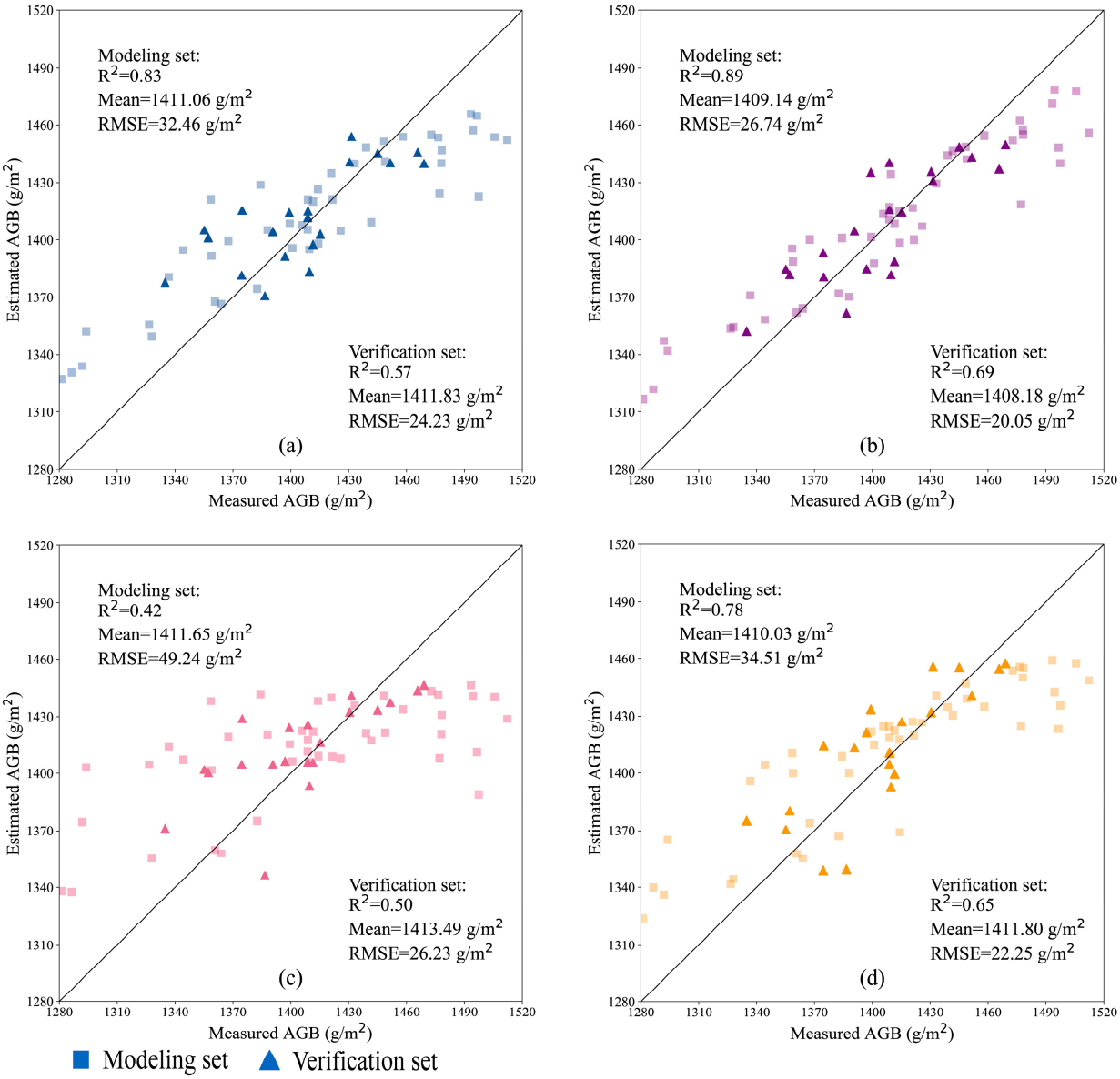

Figure 13. Simulation results of biomass with introduced terrain parameters. (**a**–**d**) represent the biomass simulation results after adding terrain parameters to the optimal time series eigenvectors of the four indices, NDMVI, SAVI, NDVI, and EVI, respectively.

4. Discussion

4.1. Advantages of Vegetation Index Time Series (VI-TS) Parameters in Enhancing Model Accuracy over Single-Time-Phase Indicators

Based on the results shown in Figure 9a–d, it is evident that the accuracy of the highland barley AGB simulation significantly improves as the growth stage advances. This suggests that the model performs better when the single-time-phase metrics used are closer to the crop sampling date. The observed trend may be attributed to various processes that occur during plant maturation, which facilitate a more efficient conversion of absorbed solar radiation, water, fertilizers, and other nutrients into AGB, especially as the plant nears the later stages of growth. A key process is the shift in the root–crown ratio during plant growth [64]. Initially, most nutrients are allocated to the roots during the early stages of growth and development. However, as the plant approaches the end of its growth cycle, nutrients are increasingly allocated to the aboveground organs, leading to a rapid

accumulation of AGB in the plant's aboveground parts. In summary, the closer the growth stage is to the crop maturity date, the better the highland barley AGB simulation results. Nonetheless, overall simulation accuracy remains low, regardless of the growth stage's single-time-phase index used. Between the second growth stage, marked by the fastest growth of vegetation leaves, and the sampling date, the AGB simulation results for each growth stage exhibit apparent saturation effects, which significantly limit the application of single-time-phase metrics in highland barley AGB simulation.

The time series parameter simulation (Figure 11) showed a notable improvement over the single-time-phase indicator (Figure 9). Integrating seasonal phenological traits of crop growth into the time series parameters significantly enhances model accuracy, surpassing the simple vegetation index single-time-phase data [24]. Our results are well supported by previous efforts in crop biomass estimation, which have demonstrated the effectiveness of multi-temporal vegetation indices and phenological data in improving yield prediction models [28,65]. The highest simulation accuracy was achieved with EVI time series parameters, while NDVI had the lowest. By combining feature selection and index importance ranking (Figure 10), EVI required only two features, Smax and INT_SOS, to attain the highest simulation accuracy across all indices. This likely relates to the physiological state of vegetation indicated by these parameters. Smax denotes the rapid growth rate of aboveground nutrient organs, such as stems and leaves, reflecting vigorous vegetation growth and their pre-flowering stage contribution to AGB. As vegetation enters the next phenological phase (Plateau), the development of these nutrient organs stabilizes. Subsequent AGB increases stem mainly from the growth of reproductive parts like seeds. INT_SOS represents the offline integral of the VI-TS curve from the season's start to the sampling date, indicating the cumulative vegetation biomass status. Huete et al. [48] found that EVI time series profiles more accurately depict various biomes' growing seasons, with seasonal curves more symmetrical around the growth peak due to their sensitivity to high biomass areas, allowing better vegetation growth monitoring. Our findings align with this. SAVI simulations, while relatively accurate, required up to seven features. Despite using time series parameters, NDVI still showed saturation effects. This may be because the data sampling period (5–15 August) was selected to minimize the impact of the high biomass phase when crop leaves begin to yellow. However, existing sampled data saturation still significantly influenced the simulations, as Prabhakara et al. [46] discussed. EVI and SAVI are less prone to rapid saturation than NDVI and can better respond to denser vegetation canopies.

4.2. Terrain Effect Enhances the Model Accuracy

In the highland barley AGB simulation that utilizes time series parameters, NDMVI demonstrates higher simulation accuracy than NDVI, indicating the potential for NDVI correction through terrain adjustment. However, recursive feature elimination results depicted in Figure 10 reveal that NDVI requires only two features, while NDMVI necessitates seven, suggesting that the accuracy gains of NDMVI over NDVI come at the cost of increased complexity—a notable disadvantage. Moreover, the terrain correction's utility for NDMVI appears limited. When compared to remote sensing indices like EVI and SAVI, which disregard terrain effects, NDMVI's benefits are not clearly superior. Consequently, it can be inferred that the accuracy improvements in AGB simulation by EVI and SAVI, which correct for soil, atmospheric, and other factors, are more substantial than those achieved through terrain factor corrections with NDMVI. This underscores the advantage of EVI and SAVI in highland barley AGB simulations, as noted by Prabhakara et al. [46]. Focusing solely on terrain or saturation effects for NDVI correction yields only marginal enhancements in highland barley AGB simulation accuracy. These findings also suggest

avenues for future research in correcting terrain factors in vegetation indices or developing new remote sensing indices.

The accuracy enhancement in highland barley AGB simulation from NDMVI's terrain correction is modest, as it fails to address both terrain and saturation effects. NDMVI primarily focuses on the terrain effect within the sampled farmland. To address this issue, the terrain shading factor, Covering_effect, was introduced to quantify the influence of surrounding terrain on crop solar radiation reception. Figure 12's feature importance ranking, post-integration into the predictive variables, indicates that this terrain parameter significantly influences the modeling of NDMVI, SAVI, and NDVI, but less so for EVI. The terrain parameter notably boosts the model accuracy for NDMVI, SAVI, and NDVI, enriching these indices' time series parameters with additional information. EVI, a non-wavelength-ratio vegetation index, inherently includes more terrain noise compared to ratio-type indices like NDVI [49]. The soil adjustment factor "L" in EVI renders it more topography-sensitive than NDVI [66], suggesting that incorporating a topographic influence factor should ideally enhance EVI's biomass monitoring precision. However, in this study, the terrain parameter Covering_effect did not positively affect EVI's simulation performance and even had a negative impact. We speculate that this is because other studies on the sensitivity of vegetation indices to terrain effects focus on terrain factors within sample plots or at VI sampling points. Correcting these factors can improve crop biomass monitoring accuracy, as demonstrated by the enhanced simulation performance of NDMVI compared to NDVI. However, in our study, given the negligible micro-topographic variations (such as slope and aspect) in most agricultural lands following the implementation of the Grain for Green Policy, the quantified Covering_effect primarily reflects the influence of surrounding terrain rather than internal terrain effects within the sampled farmland. Moreover, EVI's design is intended to mitigate atmospheric effects rather than terrain effects, which may explain why the inclusion of Covering_effect did not improve EVI's modeling performance.

In this study, the standard MODIS coefficients used for EVI calculation were not regionally optimized. Nevertheless, EVI still outperformed other indices. We attribute this to the fact that the standard coefficients provide a reasonable approximation of the atmospheric and background conditions in the study area. Additionally, EVI's inherent advantages—such as its ability to effectively reduce interference from atmospheric and soil background noise and to better capture vegetation signals in high biomass areas—make it more robust in our study region.

It is worth noting that while EVI's performance is independent of the terrain parameter Covering_effect in this study, this does not imply that terrain effects can be ignored in all cases. If there are significant topographic variations within the sampled farmland, terrain correction (whether applied to the remote sensing imagery itself or to the vegetation indices) could still play a critical role in improving the accuracy of AGB estimation.

4.3. Limitations and Prospects

The overarching objective of this study was to assess the differences, strengths, and weaknesses of time series remote sensing parameters versus single-time-phase metrics for estimating AGB, while also scrutinizing the influence of terrain factors on AGB estimation. Among these objectives, the primary focus lay on developing time series information. Although the approach involved utilizing parameters preceding the sampling date, the double logistic function fitting method employed necessitates reconstructing time series data across the entire crop growth cycle to achieve heightened temporal accuracy. When estimating AGB at a specific point within the current crop cycle, one can solely rely on preceding time series data and cannot access future time series. Consequently, a key challenge lies in reconstructing high-quality VI-TS curves. Furthermore, previous studies have

highlighted the efficacy of incorporating climatic variables such as rainfall as predictor variables to augment VI-TS curve information. Seasonal rainfall has been found to exhibit a strong correlation with crop yield and AGB [67]. However, this aspect has not been addressed here due to inadequate precipitation data availability. Kamir et al. [16] demonstrated in a study on wheat yields that climatic variables in conjunction with NDVI time series constitute effective methods for constructing large-scale yield and AGB prediction models. This insight paves the way for future research endeavors, suggesting avenues for further exploration in this domain.

5. Conclusions

This study proposes an effective approach for estimating AGB at any stage of crop growth, leveraging time series data and terrain effects to improve accuracy. The time series parameters utilized, such as phenological information and integration under the curve, do not focus on specific growth phases. The time series parameter inversion method does not rely on particular growth periods like peak growth or senescence, offering greater flexibility in selecting time points for crop AGB estimation. We observe varying degrees of saturation effects in the simulation results of single-time-phase metrics as growth stages progressed, rendering them inadequate for practical crop growth monitoring. Conversely, the use of time series parameters significantly enhances the accuracy of highland barley AGB simulations (Figure 11). Among the four vegetation indices (VIs) studied, only NDVI exhibits saturation effects, while the other three indices produced satisfactory results. Considering EVI's superior simulation accuracy, minimal feature requirements, and sensitivity to high biomass areas, we recommend employing EVI time series parameters as the primary choice for highland barley AGB simulation.

Meanwhile, we introduce NDMVI in the time series parameters study to compare the efficacy of various VIs in simulating AGB. NDMVI specifically addresses terrain effects on NDVI within agricultural plots, enhancing NDVI biomass simulation accuracy to some extent. However, it does not exhibit significant advantages over SAVI and EVI, which primarily correct for soil and atmospheric influences. It is encouraging to see that our proposed terrain factor, which considers surrounding terrain effects, significantly contributes to highland barley biomass simulation in our study area. Nevertheless, it is noteworthy that our proposed terrain parameter solely accounts for topography's influence on solar radiation during crop growth. Future investigations should delve into the effects of topography-induced variations in water distribution, fertilizer dispersal, and temperature fluctuations, as well as the microclimatic conditions it engenders, on the accuracy of highland barley AGB simulation.

Author Contributions: Conceptualization, J.H. and X.D.; methodology, J.H.; validation, J.H. and Y.S.; investigation, H.H., S.Y. and S.G.; data curation, J.H. and Y.D.; writing—original draft preparation, J.H.; writing—review and editing, X.D., Y.Z. and H.W.; visualization, J.H., J.X. (Jingyuan Xu), and J.X. (Jing Xiao); supervision, Q.L.; project administration, X.D.; funding acquisition, Q.L. All authors have read and agreed to the published version of the manuscript.

Funding: This study was funded by the National Key R&D Program of China (2021YFE0117800) and the Key Program of High-resolution Earth Observation System (00-Y30B01-9001-22/23-CY-10, 20-Y30F10-900120/22).

Data Availability Statement: The original contributions presented in this study are included in the article. Further inquiries can be directed to the corresponding author.

Conflicts of Interest: The authors declare no conflicts of interest.

References

1. Dhillon, M.S.; Dahms, T.; Kuebert-Flock, C.; Borg, E.; Conrad, C.; Ullmann, T. Modelling Crop Biomass from Synthetic Remote Sensing Time Series: Example for the DEMMIN Test Site, Germany. *Remote Sens.* **2020**, *12*, 1819. [CrossRef]
2. Jin, X.; Li, Z.; Yang, G.; Yang, H.; Feng, H.; Xu, X.; Wang, J.; Li, X.; Luo, J. Winter Wheat Yield Estimation Based on Multi-Source Medium Resolution Optical and Radar Imaging Data and the AquaCrop Model Using the Particle Swarm Optimization Algorithm. *ISPRS J. Photogramm. Remote Sens.* **2017**, *126*, 24–37. [CrossRef]
3. Santi, E.; Paloscia, S.; Pettinato, S.; Fontanelli, G.; Mura, M.; Zolli, C.; Maselli, F.; Chiesi, M.; Bottai, L.; Chirici, G. The Potential of Multifrequency SAR Images for Estimating Forest Biomass in Mediterranean Areas. *Remote Sens. Environ.* **2017**, *200*, 63–73. [CrossRef]
4. Marshall, M.; Thenkabail, P. Developing in Situ Non-Destructive Estimates of Crop Biomass to Address Issues of Scale in Remote Sensing. *Remote Sens.* **2015**, *7*, 808–835. [CrossRef]
5. Yue, J.; Yang, G.; Tian, Q.; Feng, H.; Xu, K.; Zhou, C. Estimate of Winter-Wheat above-Ground Biomass Based on UAV Ultrahigh-Ground-Resolution Image Textures and Vegetation Indices. *ISPRS J. Photogramm. Remote Sens.* **2019**, *150*, 226–244. [CrossRef]
6. Muñoz, J.D.; Finley, A.O.; Gehl, R.; Kravchenko, S. Nonlinear Hierarchical Models for Predicting Cover Crop Biomass Using Normalized Difference Vegetation Index. *Remote Sens. Environ.* **2010**, *114*, 2833–2840. [CrossRef]
7. Yang, H.; Yang, G.; Gaulton, R.; Zhao, C.; Li, Z.; Taylor, J.; Wicks, D.; Minchella, A.; Chen, E.; Yang, X. In-Season Biomass Estimation of Oilseed Rape (*Brassica napus* L.) Using Fully Polarimetric SAR Imagery. *Precis. Agric.* **2019**, *20*, 630–648. [CrossRef]
8. Dayananda, S.; Astor, T.; Wijesingha, J.; Chickadibburahalli Thimappa, S.; Dimba Chowdappa, H.; Mudalagiriyappa; Nidamanuri, R.R.; Nautiyal, S.; Wachendorf, M. Multi-Temporal Monsoon Crop Biomass Estimation Using Hyperspectral Imaging. *Remote Sens.* **2019**, *11*, 1771. [CrossRef]
9. Li, Z.; Zhao, Y.; Taylor, J.; Gaulton, R.; Jin, X.; Song, X.; Li, Z.; Meng, Y.; Chen, P.; Feng, H.; et al. Comparison and Transferability of Thermal, Temporal and Phenological-Based in-Season Predictions of above-Ground Biomass in Wheat Crops from Proximal Crop Reflectance Data. *Remote Sens. Environ.* **2022**, *273*, 112967. [CrossRef]
10. Li, Y.; Song, H.; Zhou, L.; Xu, Z.; Zhou, G. Vertical Distributions of Chlorophyll and Nitrogen and Their Associations with Photosynthesis under Drought and Rewatering Regimes in a Maize Field. *Agric. For. Meteorol.* **2019**, *272–273*, 40–54. [CrossRef]
11. Geng, L.; Che, T.; Ma, M.; Tan, J.; Wang, H. Corn Biomass Estimation by Integrating Remote Sensing and Long-Term Observation Data Based on Machine Learning Techniques. *Remote Sens.* **2021**, *13*, 2352. [CrossRef]
12. Ren, H.; Zhou, G.; Zhang, F. Using Negative Soil Adjustment Factor in Soil-Adjusted Vegetation Index (SAVI) for Aboveground Living Biomass Estimation in Arid Grasslands. *Remote Sens. Environ.* **2018**, *209*, 439–445. [CrossRef]
13. Wongchai, W.; Onsree, T.; Sukkam, N.; Promwungkwa, A.; Tippayawong, N. Machine Learning Models for Estimating above Ground Biomass of Fast Growing Trees. *Expert Syst. Appl.* **2022**, *199*, 117186. [CrossRef]
14. Zhu, X.; Liu, D. Improving Forest Aboveground Biomass Estimation Using Seasonal Landsat NDVI Time-Series. *ISPRS J. Photogramm. Remote Sens.* **2015**, *102*, 222–231. [CrossRef]
15. Zhang, B.; Zhang, L.; Xie, D.; Yin, X.; Liu, C.; Liu, G. Application of Synthetic NDVI Time Series Blended from Landsat and MODIS Data for Grassland Biomass Estimation. *Remote Sens.* **2015**, *8*, 10. [CrossRef]
16. Kamir, E.; Waldner, F.; Hochman, Z. Estimating Wheat Yields in Australia Using Climate Records, Satellite Image Time Series and Machine Learning Methods. *ISPRS J. Photogramm. Remote Sens.* **2020**, *160*, 124–135. [CrossRef]
17. Schaaf, C.B.; Li, X.; Strahler, A.H. Topographic Effects on Bidirectional and Hemispherical Reflectances Calculated with a Geometric-Optical Canopy Model. *IEEE Trans. Geosci. Remote Sens.* **1994**, *32*, 1186–1193. [CrossRef]
18. Si, Z.; Zain, M.; Li, S.; Liu, J.; Liang, Y.; Gao, Y.; Duan, A. Optimizing Nitrogen Application for Drip-Irrigated Winter Wheat Using the DSSAT-CERES-Wheat Model. *Agric. Water Manag.* **2021**, *244*, 106592. [CrossRef]
19. Xiao, X.; Zhang, Q.; Braswell, B.; Urbanski, S.; Boles, S.; Wofsy, S.; Moore III, B.; Ojima, D. Modeling Gross Primary Production of Temperate Deciduous Broadleaf Forest Using Satellite Images and Climate Data. *Remote Sens. Environ.* **2004**, *91*, 256–270. [CrossRef]
20. Scornet, E.; Biau, G.; Vert, J.-P. Consistency of Random Forests. *Ann. Statist.* **2015**, *43*, 1716–1741. [CrossRef]
21. Azzari, G.; Jain, M.; Lobell, D.B. Towards Fine Resolution Global Maps of Crop Yields: Testing Multiple Methods and Satellites in Three Countries. *Remote Sens. Environ.* **2017**, *202*, 129–141. [CrossRef]
22. Liu, J.; Shang, J.; Qian, B.; Huffman, T.; Zhang, Y.; Dong, T.; Jing, Q.; Martin, T. Crop Yield Estimation Using Time-Series MODIS Data and the Effects of Cropland Masks in Ontario, Canada. *Remote Sens.* **2019**, *11*, 2419. [CrossRef]
23. Nagy, A.; Fehér, J.; Tamás, J. Wheat and Maize Yield Forecasting for the Tisza River Catchment Using MODIS NDVI Time Series and Reported Crop Statistics. *Comput. Electron. Agric.* **2018**, *151*, 41–49. [CrossRef]
24. Bolton, D.K.; Friedl, M.A. Forecasting Crop Yield Using Remotely Sensed Vegetation Indices and Crop Phenology Metrics. *Agric. For. Meteorol.* **2013**, *173*, 74–84. [CrossRef]

25. Jiang, H.; Hu, H.; Zhong, R.; Xu, J.; Xu, J.; Huang, J.; Wang, S.; Ying, Y.; Lin, T. A Deep Learning Approach to Conflating Heterogeneous Geospatial Data for Corn Yield Estimation: A Case Study of the US Corn Belt at the County Level. *Glob. Change Biol.* **2020**, *26*, 1754–1766. [CrossRef] [PubMed]
26. Dymond, C.C.; Mladenoff, D.J.; Radeloff, V.C. Phenological Differences in Tasseled Cap Indices Improve Deciduous Forest Classification. *Remote Sens. Environ.* **2002**, *80*, 460–472. [CrossRef]
27. Dong, J.; Kaufmann, R.K.; Myneni, R.B.; Tucker, C.J.; Kauppi, P.E.; Liski, J.; Buermann, W.; Alexeyev, V.; Hughes, M.K. Remote Sensing Estimates of Boreal and Temperate Forest Woody Biomass: Carbon Pools, Sources, and Sinks. *Remote Sens. Environ.* **2003**, *84*, 393–410. [CrossRef]
28. Prasad, N.R.; Patel, N.R.; Danodia, A. Cotton Yield Estimation Using Phenological Metrics Derived from Long-Term MODIS Data. *J Indian Soc Remote Sens* **2021**, *49*, 2597–2610. [CrossRef]
29. Perry, E.; Sheffield, K.; Crawford, D.; Akpa, S.; Clancy, A.; Clark, R. Spatial and Temporal Biomass and Growth for Grain Crops Using NDVI Time Series. *Remote Sens.* **2022**, *14*, 3071. [CrossRef]
30. Tefera, A.T.; Banerjee, B.P.; Pandey, B.R.; James, L.; Puri, R.R.; Cooray, O.; Marsh, J.; Richards, M.; Kant, S.; Fitzgerald, G.J.; et al. Estimating Early Season Growth and Biomass of Field Pea for Selection of Divergent Ideotypes Using Proximal Sensing. *Field Crops Res.* **2022**, *277*, 108407. [CrossRef]
31. Xing, Z.; Wu, P.; Zhu, M.; Qian, H.; Hu, Y.; Guo, B.; Wei, H.; Xu, K.; Huo, Z.; Dai, Q.; et al. Temperature and Solar Radiation Utilization of Rice for Yield Formation with Different Mechanized Planting Methods in the Lower Reaches of the Yangtze River, China. *J. Integr. Agric.* **2017**, *16*, 1923–1935. [CrossRef]
32. Manevski, K.; Lærke, P.E.; Jiao, X.; Santhome, S.; Jørgensen, U. Biomass Productivity and Radiation Utilisation of Innovative Cropping Systems for Biorefinery. *Agric. For. Meteorol.* **2017**, *233*, 250–264. [CrossRef]
33. Riihimäki, H.; Heiskanen, J.; Luoto, M. The Effect of Topography on Arctic-Alpine Aboveground Biomass and NDVI Patterns. *Int. J. Appl. Earth Obs. Geoinf.* **2017**, *56*, 44–53. [CrossRef]
34. Mahler, R.L.; Bezdicek, D.F.; Witters, R.E. Influence of Slope Position on Nitrogen Fixation and Yield of Dry Peas. *Agron. J.* **1979**, *71*, 348–351. [CrossRef]
35. Kravchenko, A.N.; Bullock, D.G. Correlation of Corn and Soybean Grain Yield with Topography and Soil Properties. *Agron. J.* **2000**, *92*, 75–83. [CrossRef]
36. Zellweger, F.; Braunisch, V.; Morsdorf, F.; Baltensweiler, A.; Abegg, M.; Roth, T.; Bugmann, H.; Bollmann, K. Disentangling the Effects of Climate, Topography, Soil and Vegetation on Stand-Scale Species Richness in Temperate Forests. *For. Ecol. Manag.* **2015**, *349*, 36–44. [CrossRef]
37. Wei, H.; Lyu, C.; Yin, X. Spatial differentiation of farmland and influencing factors on the Qinghai-Tibet Plateau. *Sci. Geogr. Sin.* **2023**, *43*, 379–387. [CrossRef]
38. Shi, W.; Lu, C.; Shi, X.; Cui, J. Patterns and Trends in Grain Self-Sufficiency on the Tibetan Plateau during 1985–2016. *J. Geogr. Sci.* **2020**, *30*, 1590–1602. [CrossRef]
39. Wang, C.-Y.; Song, Y.-L.; Linderholm, H.W.; Li, Y.; Zhang, B.-T.; Du, J.; Li, F.-X.; Wang, M.-T.; Wang, R.-Y.; Zhu, Y.; et al. The Influence of Increasing Temperatures on Highland Barley Yields and on the Maximum Cultivation Altitude on the Tibetan Plateau. *Adv. Clim. Change Res.* **2023**, *14*, 573–579. [CrossRef]
40. Cossani, C.M.; Slafer, G.A.; Savin, R. Yield and Biomass in Wheat and Barley under a Range of Conditions in a Mediterranean Site. *Field Crops Res.* **2009**, *112*, 205–213. [CrossRef]
41. Ma, W.; Jia, W.; Su, P.; Feng, X.; Liu, F.; Wang, J. Mapping Highland Barley on the Qinghai–Tibet Combing Landsat OLI Data and Object-Oriented Classification Method. *Land* **2021**, *10*, 1022. [CrossRef]
42. Zhao, Y.; Wang, Y.; Xu, X.; Dong, L. Effect of the Asian Water Tower over the Qinghai-Tibet Plateau and the Characteristics of Atmospheric Water Circulation. *Chin. Sci. Bull.* **2019**, *64*, 2830–2841. [CrossRef]
43. Du, X.; Li, Q.; Zhao, L.; Shen, Y.; Zhang, S.; Zhang, Y.; Wang, H.; Xu, J. Identification of Cropland in Tibetan Plateau Based on Time Series Remote Sensing Features. *Geocarto Int.* **2024**, *39*, 2375583. [CrossRef]
44. Wang, J.; Li, H.; Yang, L.; Li, Y.; Wei, B.; Yu, J.; Feng, F. Distribution and Translocation of Selenium from Soil to Highland Barley in the Tibetan Plateau Kashin-Beck Disease Area. *Env. Geochem Health* **2017**, *39*, 221–229. [CrossRef] [PubMed]
45. Zeng, X.; Guo, Y.; Xu, Q.; Mascher, M.; Guo, G.; Li, S.; Mao, L.; Liu, Q.; Xia, Z.; Zhou, J.; et al. Origin and Evolution of Qingke Barley in Tibet. *Nat Commun* **2018**, *9*, 5433. [CrossRef] [PubMed]
46. Prabhakara, K.; Hively, W.D.; McCarty, G.W. Evaluating the Relationship between Biomass, Percent Groundcover and Remote Sensing Indices across Six Winter Cover Crop Fields in Maryland, United States. *Int. J. Appl. Earth Obs. Geoinf.* **2015**, *39*, 88–102. [CrossRef]
47. Xue, J.; Su, B. Significant Remote Sensing Vegetation Indices: A Review of Developments and Applications. *J. Sens.* **2017**, *2017*, 1353691. [CrossRef]
48. Huete, A.; Didan, K.; Miura, T.; Rodriguez, E.P.; Gao, X.; Ferreira, L.G. Overview of the Radiometric and Biophysical Performance of the MODIS Vegetation Indices. *Remote Sens. Environ.* **2002**, *83*, 195–213. [CrossRef]

49. Zhu, G.L.; Liu, Y.B.; Ju, W.M.; Chen, J.M. Evaluation of Topographic Effects on Four Commonly Used Vegetation Indices. *J. Remote Sens.* **2013**, *17*, 210–234.
50. Roupioz, L.; Jia, L.; Nerry, F.; Menenti, M. Correction of Sub-Pixel Topographical Effects on Land Surface Albedo Retrieved from Geostationary Satellite (FengYun-2D) Observations. *IOP Conf. Ser. Earth Environ. Sci.* **2014**, *17*, 012270. [CrossRef]
51. Yu, W.; Li, J.; Liu, Q.; Yin, G.; Zeng, Y.; Lin, S.; Zhao, J. A Simulation-Based Analysis of Topographic Effects on LAI Inversion Over Sloped Terrain. *IEEE J. Sel. Top. Appl. Earth Obs. Remote Sens.* **2020**, *13*, 794–806. [CrossRef]
52. Wu, Z.; Xu, H. A New Index for Vegetation Enhancements of Mountainous Regions Based on Satellite Image Data: A New Index for Vegetation Enhancements of Mountainous Regions Based on Satellite Image Data. *Geo-Inf. Sci.* **2011**, *13*, 656–666. [CrossRef]
53. Rouse, J.W., Jr.; Haas, R.H.; Deering, D.; Schell, J.; Harlan, J.C. *Monitoring the Vernal Advancement and Retrogradation (Green Wave Effect) of Natural Vegetation*; NASA: Washington, DC, USA, 1974.
54. Miura, T.; Huete, A.R.; Yoshioka, H. Evaluation of Sensor Calibration Uncertainties on Vegetation Indices for MODIS. *IEEE Trans. Geosci. Remote Sens.* **2000**, *38*, 1399–1409. [CrossRef]
55. Huete, A.R. A Soil-Adjusted Vegetation Index (SAVI). *Remote Sens. Environ.* **1988**, *25*, 295–309. [CrossRef]
56. Teijido-Murias, I.; Barrio-Anta, M.; López-Sánchez, C.A. Evaluation of Correction Algorithms for Sentinel-2 Images Implemented in Google Earth Engine for Use in Land Cover Classification in Northern Spain. *Forests* **2024**, *15*, 2192. [CrossRef]
57. FREI, W. Understanding Anisotropic Reflectance in Mountainous Terrain. *Photogramm. Eng. Remote Sens.* **1983**, *49*, 671–683.
58. Fisher, J.; Mustard, J.; Vadeboncoeur, M. Green Leaf Phenology at Landsat Resolution: Scaling from the Field to the Satellite. *Remote Sens. Environ.* **2006**, *100*, 265–279. [CrossRef]
59. Zhang, X.; Friedl, M.A.; Schaaf, C.B.; Strahler, A.H.; Hodges, J.C.F.; Gao, F.; Reed, B.C.; Huete, A. Monitoring Vegetation Phenology Using MODIS. *Remote Sens. Environ.* **2003**, *84*, 471–475. [CrossRef]
60. Zhu, W.; He, B.; Xie, Z.; Zhao, C.; Zhuang, H.; Li, P. Reconstruction of Vegetation Index Time Series Based on Self-Weighting Function Fitting from Curve Features. *Remote Sens.* **2022**, *14*, 2247. [CrossRef]
61. Liu, L.; Cao, R.; Chen, J.; Shen, M.; Wang, S.; Zhou, J.; He, B. Detecting Crop Phenology from Vegetation Index Time-Series Data by Improved Shape Model Fitting in Each Phenological Stage. *Remote Sens. Environ.* **2022**, *277*, 113060. [CrossRef]
62. Xie, C.; Wang, J.; Peng, W.; Zhang, K.; Liu, J.; Yu, B.; Jiang, X. The New Round of CCFP: Policy Improvement and Implementation Wisdom—Based on the Results of Social and Economic Benefit Inventory of CCFP in 2015. *For. Econ.* **2016**, *38*, 43–51+81. [CrossRef]
63. Powell, S.L.; Cohen, W.B.; Healey, S.P.; Kennedy, R.E.; Moisen, G.G.; Pierce, K.B.; Ohmann, J.L. Quantification of Live Aboveground Forest Biomass Dynamics with Landsat Time-Series and Field Inventory Data: A Comparison of Empirical Modeling Approaches. *Remote Sens. Environ.* **2010**, *114*, 1053–1068. [CrossRef]
64. Amos, B.; Walters, D.T. Maize Root Biomass and Net Rhizodeposited Carbon: An Analysis of the Literature. *Soil Sci. Soc. Am. J.* **2006**, *70*, 1489–1503. [CrossRef]
65. Sehgal, V.K.; Rajak, D.R.; Chaudhary, K.N.; Dadhwal, V.K. Improved Regional Yield Prediction by Crop Growth Monitoring System Using Remote Sensing Derived Crop Phenology. *Int. Arch. Photogramm. Remote Sens. Spat. Inf. Sci.* **2002**, *34*, 329–334.
66. Matsushita, B.; Yang, W.; Chen, J.; Onda, Y.; Qiu, G. Sensitivity of the Enhanced Vegetation Index (EVI) and Normalized Difference Vegetation Index (NDVI) to Topographic Effects: A Case Study in High-Density Cypress Forest. *Sensors* **2007**, *7*, 2636–2651. [CrossRef] [PubMed]
67. Waldner, F.; Horan, H.; Chen, Y.; Hochman, Z. High Temporal Resolution of Leaf Area Data Improves Empirical Estimation of Grain Yield. *Sci. Rep.* **2019**, *9*, 15714. [CrossRef]

Disclaimer/Publisher's Note: The statements, opinions and data contained in all publications are solely those of the individual author(s) and contributor(s) and not of MDPI and/or the editor(s). MDPI and/or the editor(s) disclaim responsibility for any injury to people or property resulting from any ideas, methods, instructions or products referred to in the content.